LT-0400 OTDR - Optical Time Domain Reflectometer

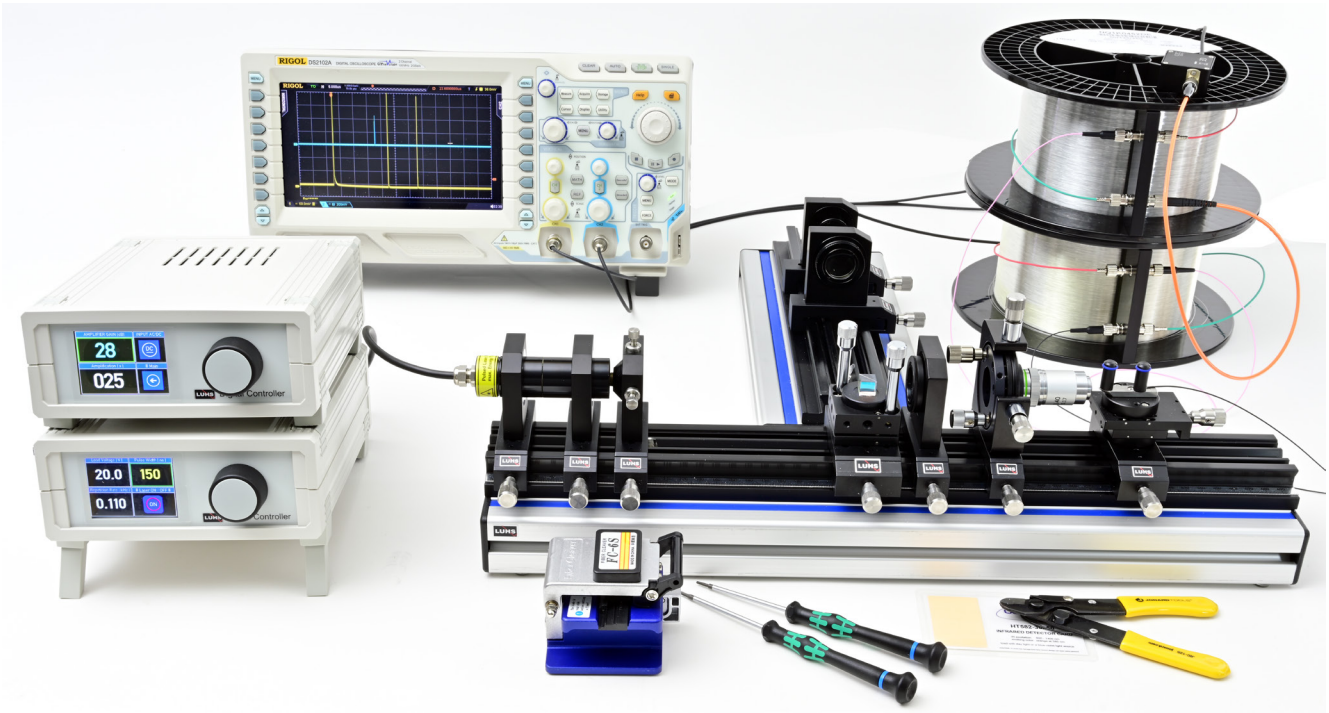

Table of Contents

1.0 Introduction

When Javan and his colleagues discovered the first laser in the year 1960, it was considered as an academic curiosity. Today it is difficult to encompass the bandwidth of the applications of lasers in a few words. The cutting of several cm thick steel plates, the construction of structures with an accuracy in the realm of nanometre, demonstrate very distinctly the lasers multiple possibilities while working on materials. The property of lasers used here is the high radiation power, which by the focusing of the beam diameter to low some mm leads to extremely high intensities. Of the many, the most frequent applications of the laser are not based on its radiation power, but rather on its focussing capability.

The words that you are reading here, have been printed by a Laser printer. While reading these lines, you may prefer to hear the playback of a CD, with the realisation that here also the laser plays a very important role, with the focussing capability of the laser diode of the radiation being foremost. When one sees the numbers of lasers produced yearly, the figures of laser diodes produced, far exceed the other numbers by a large margin. An equally large field of application of laser diodes is in the News Media technique where the transmitted information consisting of modulated laser light is transported thousands of kilometres by the use of optical fibres. It should be kept in mind that as soon as an improved laser is developed in the production of laser diodes, it enters the cycle of further refinements.

Another not so common application of the laser is found in measurement techniques. These applications utilise the high monochromatic property of the laser, with the precise definition of the wavelength as a tool for the measurement of length. One measures an object in units from the wavelength which are translated to a definite co-relation on the measuring meter. A basic type of such measuring instrument is the Michelson Interferometer which utilises the interference capability of coherent laser light.

There exist a whole series of measurement problems which cannot be resolved by the above mentioned methods. Typical characteristic problems of measurement tasks is the comparatively large distance to the object being examined. Michelson Interferometers cannot be used in this case, because they are based on a more or less precise linear movement of the measuring reflectors. Above all, it is important that the reflector is lead from a zero point till the object without interruption of the laser beam. For further convenience, a method has been developed by which the transit time of a laser pulse to the object and back can be measured. In principle, this technique by itself is not new. It has been used since long for Echo Sound Measurement with Ultrasonics or in Radar technique. Whether Ultrasonics or radio waves can be collimated to a low divergent beam as it can be done with lasers.
The purpose is mostly to determine the distance to a possibly sharply localized object. For example; when the distance to a church tower top or the distance to the moon has to be actually measured with the laser.
Determining the speed of objects can be performed with the co-relation of multiple distance determinations over time. Unpopular applications are for example; Laser radar of the police to overtake fast drivers. Exactly opposite to the Radar system, singular and definite vehicles in a lot of traffic can also be selected. In this sense the word „ Laser radar“ is a wrong combination, because Radar stands for Radio-wave Detection and Ranging. Therefore the introductory description as LIDAR is better and stands for Light detection and ranging
A further important application field of the echo measurement was and is even today the Time Domain Reflectometry. By this technique, an electrical impulse is sent through a copper wire and the returning echoes measured. Echoes can only originate when the pulse is reflected from an irregular centre or imperfection. In this way one also has the facility to localise the defective spots in a cable and effect the required repairs. The increasing world-wide shift of the news cable media from Copper to Glass fibres makes such an apparatus necessary which is now known as:

OTDR

(optical time domain reflectometer). Even here, the transit time of the light to a fault spot is measured and thus permits the localization of the interference. Both techniques add to the application of the LIDAR, the first one in a free field and the second to be carried out within a glass fibre. Within the framework of this experiment, both methods shall first be theoretically described and thereafter tested in the laboratory.

2.0 Fundamentals

2.1 Basics of LIDAR

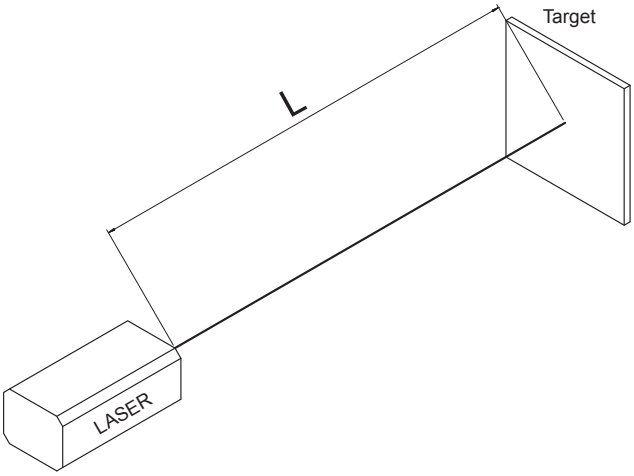

Fig. 1: Principle of transit time measurement

At the distance L, we find the object to be measured. The time Δt that a laser pulse requires in order to return from the object to the laser is:

$$\Delta t = 2 \cdot \frac{L}{v} = 2 \cdot \frac{n \cdot L}{c} \qquad \textbf{(1)}$$

Where v is the speed of the laser pulse, n the refractive index of the surrounding air and c is the speed of light in a vacuum. The refractive index of air is mainly determined through its density, which on the other hand is dependent on air pressure, temperature and its composition. The common formula for the calculation of the refractive index of air as a function of the air pressure P (in hPa) and the temperature u (in °C) originates from Edlén and has become the standard for dry air:

$$(n-1)_{p,\upsilon} = 2.8775 \cdot 10^{-7} \cdot P \cdot \frac{1 + 10^{-6} \cdot P \cdot (0.613 - 0.00997 \cdot \upsilon)}{1 + 0.003661 \cdot \upsilon}$$

Water content in air has an influence on the refractive index n. The relative humidity *RF* (in %) leads to the reduction of the refractive index and thus for standard humid air, it results in an additional term:

The derivation of the refractive index thus depends on the following parameters:

$$\frac{dn}{d\upsilon} = -0.93 \cdot 10^{-6} \left[K^{-1} \right]$$

$$\frac{dn}{dP} = +0.27 \cdot 10^{-6} \left[hPa^{-1} \right]$$

$$\frac{dn}{dRF} = -0.96 \cdot 10^{-8} \left[\%^{-1} \right]$$

An error in estimation results from the total of the differential relationship for the determination of the distance L.

$$L = \frac{c}{2 \cdot n} \cdot \Delta t$$

the relative error:

$$\frac{dL}{L} = \left| \frac{dn}{n} \right| + \left| \frac{d\Delta t}{t} \right| \qquad \textbf{(2)}$$

The speed of light in a vacuum as per the definition is error free. With (2) the relative error for the determination of the distance with different values for air pressure, air temperature, the relative humidity and the precise time measurement can be calculated for the respective measuring task.
After these fundamental considerations, the construction according to Fig. 1 should now be improved progressively so as to achieve in the end a technically meaningful instrument.

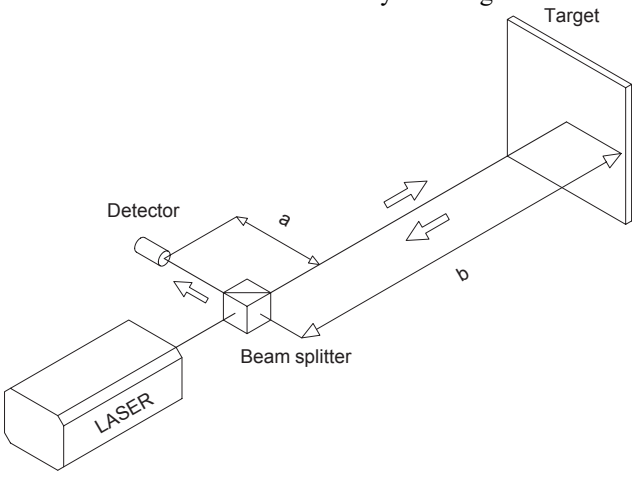

Fig. 2: Transit time measurement with detector

In practice, a construction according to Fig. 2 is used. Here one sets up the total length L as the sum of the paths a and b. The path a is in general a set-up constant which then merits consideration only if b is not very larger as a**.** The laser beam traverses through a beam splitter which alters the output corresponding to the dividing proportion. A part of the returning laser beam hits the detector. As there is no ideal beam splitter, a part of the laser beam in the passage through the beam splitter also comes in contact with the detector. One therefore gets the initial starting impulse for time measurement**.** Assuming the refractive index of the atmosphere to be 1 and the distance to the target object to be 1 m, one derives the transit time of Δt from:

$$\Delta t = \frac{2}{3 \cdot 10^8} = 6.7 \text{ nsec}$$

In order to achieve a separation of the initial starting impulse and the echo impulse at the detector, the laser pulse must be smaller than this value. Now the essential interest does not lie in the inclusion of smaller distances, but a lot more in the measurement of larger distances within the region of some kilometre. This however, demands a laser beam, which can also remain almost parallel over these large distances. Typical data for the divergence (He Ne Laser) are for e.g. 1 mrad. This value means that the diameter of the laser beam enlarges itself to approx. 2mm per meter of distance. The initial diameter of 1 mm results in the diameter of approx. 200 mm over a distance of 100 m.

2.2 Gaussian Beams

In reality, there are no actual parallel light bundles and even wave fronts also exist only at particular points. The main reason for the failure of the geometrical optics lies in the fact that they were established at a time when one still did not know that light is an electromagnetic wave and that its behaviour can be described using the Maxwell equation. For this we use here the known wave equation. :

$$\Delta \vec{E} - \frac{n^2}{c^2} \cdot \frac{\partial^2 \vec{E}}{\partial t^2} = 0$$

Without restrictions light would spread itself in all directions in space as a spherical wave.

$$\vec{E} = \vec{E}(r) \text{ with } r^2 = x^2 + y^2 + z^2$$

If, however we are interested in the technically important case of the spherical wave spreading in direction z in a small solid angle then the solution is an equation for the electrical field.

$$\vec{E} = \vec{E}(r,z) \text{ with } r^2 = x^2 + y^2 + z^2$$

The solution to the wave equation is found in fields which show a Gaussian shaped intensity distribution over the radiation cross-section and are therefore called Gaussian beams. Similar to the solution for the fibre, Gaussian beams exist according to the particular boundary conditions in different modes.
Such beams, especially the Gaussian fundamental mode (TEM_{00}) are preferably produced by lasers. However, the light coming from any light source can be seen as a superimposition of many such Gaussian modes. But the intensity of a pure mode is very small compared to the total intensity of a light source. The situation with the laser is different, where the total light intensity can be produced in the basic mode alone. This, as well as the monochromatic nature of the laser radiation, is the main difference compared to the conventional light sources.

A Gaussian beam always has a beam waist. The beam radius w is derived from the solution of the wave equation as:

$$w(z) = w_0 \cdot \sqrt{1 + \left(\frac{z}{z_R}\right)^2}$$

w_0 is the smallest beam radius of the beam waist and z_r represents the Rayleigh length.

$$z_R = w_0^2 \frac{\pi}{\lambda}$$

Fig. 3 shows the passage of the beam diameter which is dependent on the wave length z . The beam spreads itself in the z-direction. At the point where $z = z_0$ the beam has the smallest radius.

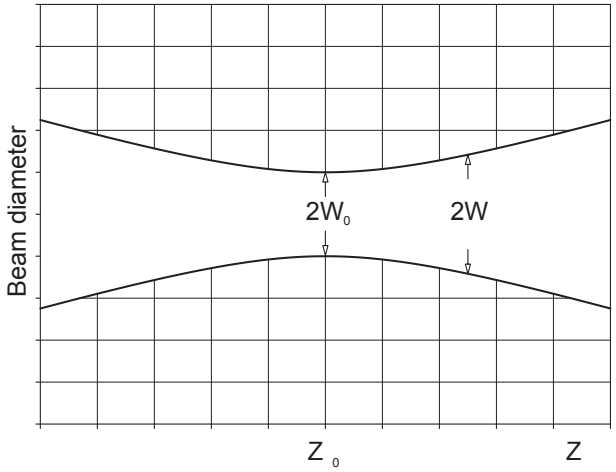

Fig. 3: Beam diameter of a Gaussian beam of TEM_{00} mode versus location z.

As the interval increases, the beam radius increases linearly. Since Gaussian beams are spherical waves, there is a radius of curvature of the wave front for every point z. The radius of the curvature R can be calculated with the following equation:

$$R(z) = z + \frac{z_r^2}{z}$$

This inter-relation is again given in the Fig. 4 where $z = z_r$ (the radius of the curvature has a minimum value) and R increases by 1/z compared to $z = 0$. With $z=0$ the radius of curvature is infinite. The wave front is plane at this juncture. The radius increases again linearly above the Rayleigh length z_r. This statement is of fundamental importance. It states that a parallel beam can only exist at one point of a light wave and that too at its focal point.

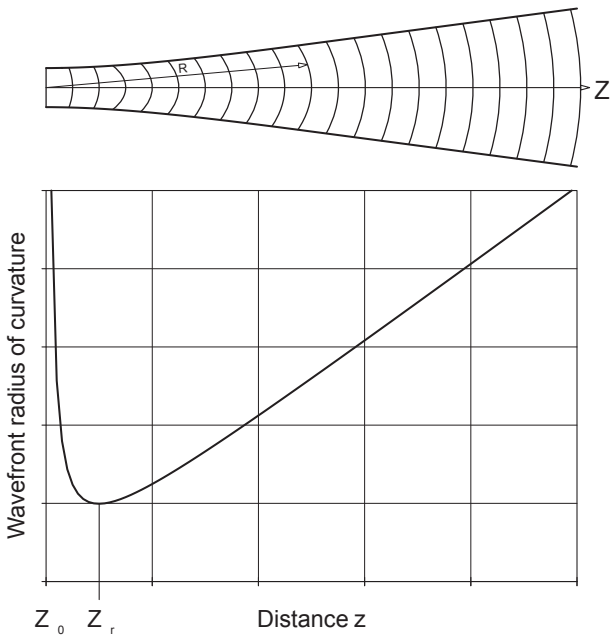

Fig. 4: Course of radius of curvature of the wave front as a function of the distance from the beam waist with z=0

In the region for

$$-z_r \le z \le z_r$$

a beam can be seen as approximately parallel or also as collinear. In the Fig. 5 Rayleigh region is shown as well as the divergence Θ in the far field region, i.e. $z>>z_0$.

The graphical representations suggest that one of the significant properties of laser beams, i.e. their lack of divergence, cannot be depicted in this way.

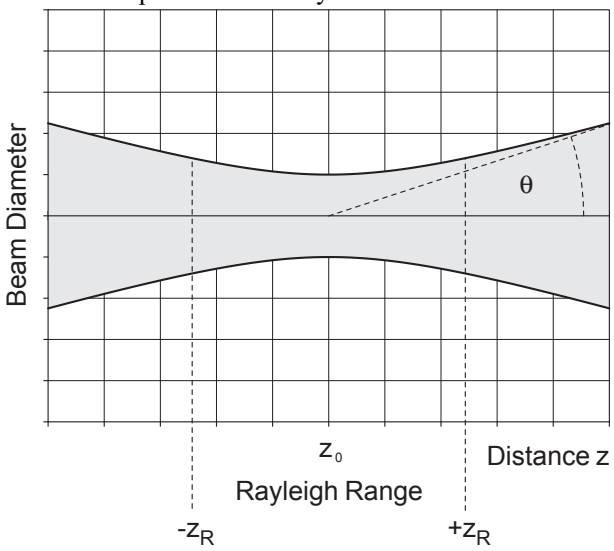

Fig. 5: Rayleigh region z_R and Divergence Θ in the far field region, $z>>z_0$

This is because the relationship of the beam diameter to z in the graph has not been normalised. If we assume as an example a HeNe-Laser (632 nm) with a beam radius of $w_o = 1$ mm at the exit of the laser, we get the value for the Rayleigh range 2 z_r :

$$2 \cdot z_R = 2w_0^2 \frac{\pi}{\lambda} = 2 \cdot 10^{-6} \frac{3.14}{623 \cdot 10^{-9}} = 9{,}9\ m$$

For our application usage, we are interested in the diverging angle Θ, which is determined from Fig. 5 as:

$$\tan\Theta = \frac{w_0}{z_r}$$

Hereby we are using the approximation that in the Rayleigh range the laser beam with radius w_0 can be considered as parallel. If we additionally use:

so we finally get:

$$\tan\Theta = \frac{\lambda}{\pi \cdot w_0} \qquad (3)$$

2.2.1 Beam expansion

The Eq. (3) clearly shows how one can effect the divergence of a Gaussian and a laser beam respectively. The smaller the wavelength λ, the smaller is the divergence. This parameter is however limited by the service quality of the laser. However, the variation of the beam radius anyhow enables a change in the divergence. In order to increase the beam diameter, one uses the expansion system which is shown in Fig. 6.

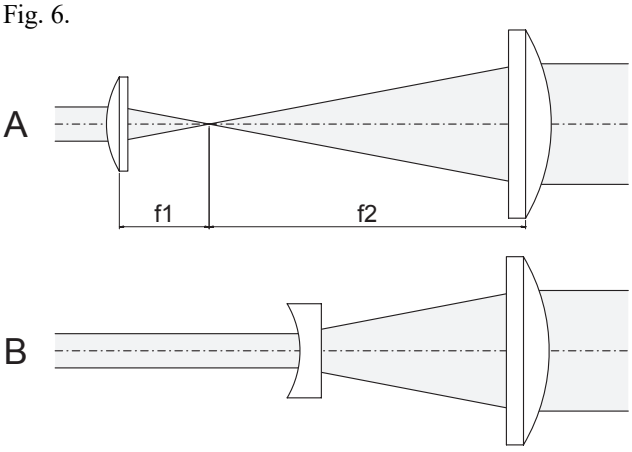

Fig. 6: Astronomical (A) and Gallilei telescope (B)

In the case of (A) two lenses with positive focal lengths are used. This arrangement from the astronomical telescope is shown here. In the second case (B) as a leading lens, one with a negative focal length is used. In both cases, the initial beam diameter d is enlarged to the final diameter D.

The advantage of the arrangement B is that the overall length is clearly smaller than it is in the case of A. In the astronomical arrangement (A) a focus originates between both the lenses. At this point one can insert a diaphragm, whose diameter is selected such a way that it is the approximate size of the beam diameter of the Gaussian fundamental mode.

All other modes have a larger diameter in focus and can therefor not pass the telescope. This diaphragm is a simple pinhole and is referred to as a spatial filter. With this type of telescopic arrangement, fitted with a spatial filter, one can refine a beam which is contaminated through dust particles on the lenses and on the exit window of the laser. Naturally, such a space filter also improves upon the divergence.

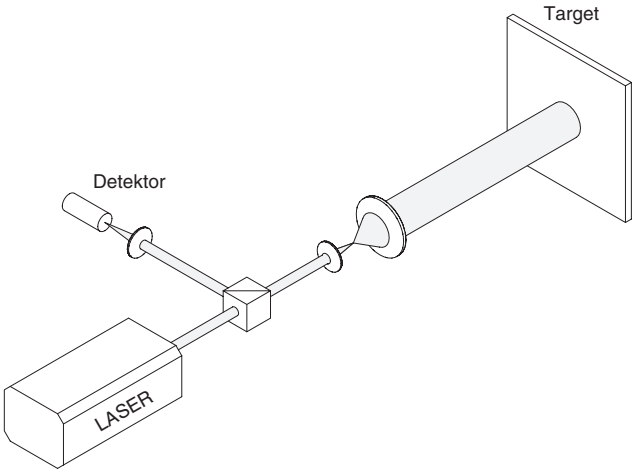

Fig. 7: Assembly of an expanding system

In the expanding system, one uses a lens combination with focal lengths of 20 and 60 mm. This leads to a reduction in the divergence around the factor 3. With the measures which have been shown till now, we are in a position to optimise the optical part of the transmitter**.**

The next step is the selection of a suitable laser. The laser should be able to emit short light pulses in the nsec region with an adjustable repetition rate. The required output depends on the respective application area. With this, the desired distance to the target object as well as the back scattering properties of the object play an important role. Now prior to the final selection of the laser, an immediate estimation is to be made of the quantity of available light scattered back from the target object. In this context, the absorption loss in the measured length as well as the sensitivity of the detector should be taken into consideration. Indeed, the estimation of the returning scattered light from the target object should be first considered. Without any doubt, this value depends on the properties of the target object. However, it is possible to compare the back scattering behaviour for many target surfaces with that of the Lambert's radiators. Such a type of radiator emits the received light according to the cosine distribution, so that it can be designated as a Cosine radiator Fig. 8

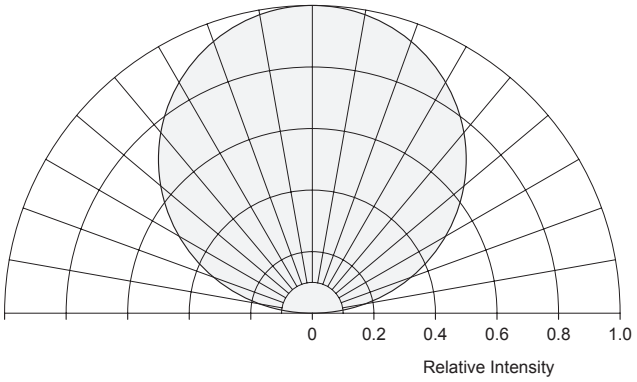

Fig. 8: Lambert's Cosine radiator

The main direction of the radiation is perpendicular to the surface of the object. Whenever possible one must therefore target the object in such a way, that this direction coincides with the measurement axis of the range meter. In reality the object distance L would be very large compared to the aperture of the telescope. Therefore one can consider the radiator as emitter of spherical waves whose intensity decreases with the quadrate of the distance L and according to the cosine distribution. The power which finally reaches

the photodetector is after all, just the power which enters through the area of the input lens. The exact formulation results in:

$$P = \beta \cdot P_0 \cdot \int_{d\Omega} \cos(\vartheta) \cdot d\Omega \qquad \textbf{(4)}$$

In which β is a constant which characterises the reflectivity of the object. With the sufficiently large distance, the input lens receives almost only light from a radiator, which originates within the angle $\vartheta \approx 0$. Consequently, Eq. (4) is simplified to:

$$P = \beta \cdot P_0 \cdot \int_{d\Omega} d\Omega = \beta \cdot P_0 \cdot \Delta\Omega$$

The angle ΔΩ is given by the solid angle of the telescope in which the radiation is picked up.

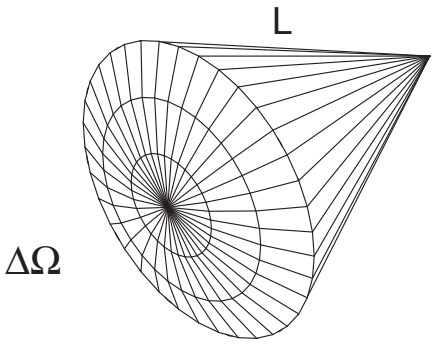

Fig. 9: Solid angle of received radiation

The radiator (target) emits radiation only in a half-sphere as it does not radiate from the rear. Therefore the ratio of the spherical segment area of the telescope to the surface of the half-sphere is directly proportional to the ratio between the received output and the radiated output:

$$\frac{2 \cdot \Delta\Omega}{\Omega} = \frac{F_{lens}}{2 \cdot \pi \cdot L^2} = \frac{P}{\beta \cdot P_0},$$

or

$$P = \beta \cdot P_0 \cdot \frac{F_{lens}}{2 \cdot \pi \cdot L^2} = \gamma \cdot P_0 \cdot \frac{r^2}{L^2}, \quad (\gamma = \beta/2) \qquad \textbf{(5)}$$

The received power P decreases to the quadrate to the distance L of the target object and it increases with the increase of the lens diameter r.

However, further loss mechanisms must also be considered. In addition, there are scattering and absorption losses. Interfering dust or water droplet particles having dimensions substantially larger than the wavelength of the laser come into question. Under such circumstances, it is not possible to carry out a reasonably accurate measurement. Therefore, one can only carry out proper measurements in clean air, which however do have absorption losses. Losses of this type can be explained and compensated for by Lambert-Beer Absorption Law:

$$P = P_0 \cdot e^{-\alpha \cdot 2 \cdot L} \qquad \textbf{(6)}$$

With this α is the absorption coefficient of the air and 2L is the total path of the radiation from the laser to the target object and back. The equation Eq. 6 is valid only when the laser wavelength is selected such that no resonance lines of gases contained in the air are excited. However, if one is interested in the composition of the air only for the sake of environmental protection an apparatus similar to the range meter but with a selected wavelength and known distance L is used. From the combination of Eq. 5 and Eq. 6 we finally get:

$$P = \gamma \cdot P_0 \cdot \frac{r^2}{L^2} \cdot e^{-2\alpha L} \qquad \textbf{(7)}$$

Eq. 7 allows us the approximate assessment of the expected power to be received. It however represents just an approximation as the parameters α and γ are dependent on other influences. Instead of relying on empirically derived parameters or Table values, practical attempts give swifter and more accurate results.

This is especially true for the usage of laser diodes with such wavelengths for which such table values are not yet available.

2.3 Triple reflector

One does not always have the possibility in the choice and selection of target objects, laser wavelengths or laser outputs. With the work of measurement being left to the installing of optical reflectors, a lot of essential tasks would become easier because then nearly the total optical output can be reflected back. A particularly suitable such a reflector is the triple mirror which has been explained in the following paragraph.

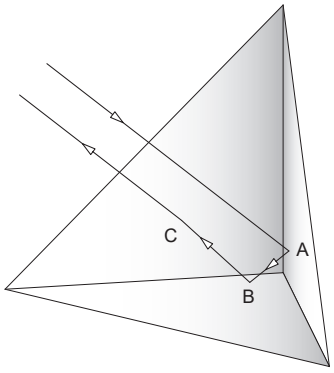

Fig. 10: Triple reflector

One cuts the corner from a hollow quadratic cube and coats the inner surfaces, thus achieving in this manner the important optical components of a triple reflector. Every light beam entering under any angle the cube corner, experiences three reflections and is finally reflected back in the same direction Fig. 10. Between the entering and exiting beams there occurs an offset which is dependent on the beam entry point into the triple reflector. One can similarly cut a corner from a cube which is completely made of glass Fig. 11. This results in reflection through total reflection. These types of triple reflectors are most frequently used. The advantage being that the reflecting surfaces are protected against dust and contamination.

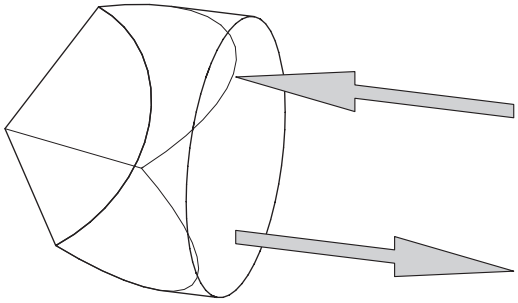

Fig. 11: Triple reflector made from Glass

A laser beam from any distance impinges on the triple reflector and provided that the beam diameter is not larger than the entrance surface of the reflector, is almost completely reflected back without losses. In order to convince oneself about the working effect of a triple reflector, a glance into it from various angles always enables one to see only one's own eyes.

2.4 Photodetector

Semiconductor pn - transitions with a band gap of E_g are suitable for the detection of optical radiation if the energy E_p of the photons is equal or greater than the band gap.

$$E_p = \hbar\omega \geq E_g$$

In this case an arriving photon can stimulate an electron to pass from the valence band to the conduction band Fig. 12.

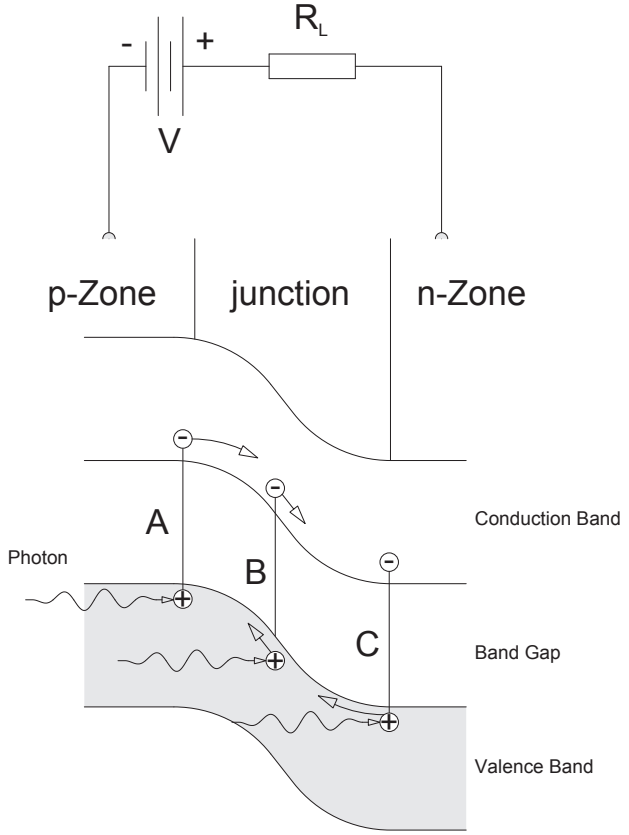

Fig. 12: Fig. 12: Absorption of a photon with subsequent transition of the stimulated electron from the valence band to the conduction band

Here three types of events are possible:

A An electron of the valence band in the p-zone is stimulated and enters the p-zone of the conduction band. Because of the external electric field due to the voltage V it will diffuse through the barrier layer into the n-zone and contributes to the external current passing the resistor R_L unless it recombines in the p-zone.

B If an electron of the barrier layer is hit by a photon the hole of the barrier layer will migrate into the p-zone and the electron into the n-zone. The drift of both charges through the barrier layer causes a current impulse. The duration of the impulse depends on the drift speed and on the length of the barrier layer.

C The case is similar to case A. The hole migrates due to the presence of the external field into the p-zone or recombines in the n-zone.

Only electrons which are in the barrier layer (case B) or near the boundary of the barrier layer (area of diffusion, case A and C) contribute to the external current due to stimulation by photons. All others will recombine within their area. In the utmost case one elementary charge q can be created for each incoming photon. As already mentioned, not every photon will create in the average a current impulse. In this context the production rate G, leading to an average current $\langle i_{Ph} \rangle$ is defined as follows:

$$\langle i_{Ph} \rangle = q \cdot G$$

At a light energy of P_0 a number of photons will hit the detector as is just the energy of one photon. But only that fraction of photons is converted into current pulses which is absorbed in the barrier layer. This fraction may be called

$\eta \cdot P_0$, where η is called quantum efficiency. The number of generated current pulses or the production rate will be

$$G = \frac{\eta}{\hbar\omega} \cdot P_0$$

and the average photo current:

$$\langle i_{Ph} \rangle = \frac{\eta \cdot q}{\hbar\omega} \cdot P_0$$

Because of processes which are typical for semiconductors there is already a current flowing even if there are no photons entering the detector. This current is called „dark" current and has four reasons:

1. Diffusion current, it is created because of statistical oscillations of the charge carriers within the diffusion area

2. Regeneration or recombination current, it is generated by random generation and annihilation of holes

3. Surface currents, which are hardly avoidable since the ideal insulator does not exist

4. Avalanche currents are flows of electrons which appear at high electric field strengths, if, for example, a high voltage is applied to the photodiode

All these effects contribute to the dark current i_D in a way that finally the characteristic line of the diode can be expressed as follows:

$$i = i_s \left(e^{\frac{q \cdot U_D}{kT}} - 1 \right) - \langle i_{Ph} \rangle = i_D - \langle i_{Ph} \rangle$$

This current i passes the load resistor R_L and provokes the voltage drop U_a, which represents the signal.

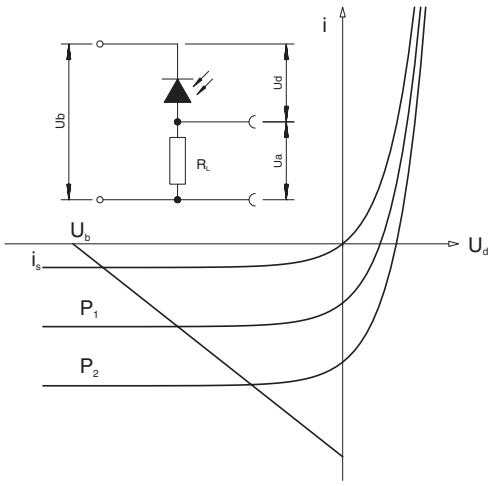

Fig. 13: Characteristic line of a photodiode in the photo conductive mode

$$i = i_s\left(e^{\frac{q}{kT}U_d} - 1\right) - \langle i_{Ph}\rangle = \frac{U_a}{R_L}$$

A good detector of optical communication technology is characterised by the fact that it is very fast (up to the GHz range) and that it has a high quantum efficiency which means that it is very sensitive. Depending on the wavelength range which has to be covered by the detector one uses silicon or germanium semiconductor material for the construction of the detectors.

2.5 Germanium and Silicon PIN-diodes

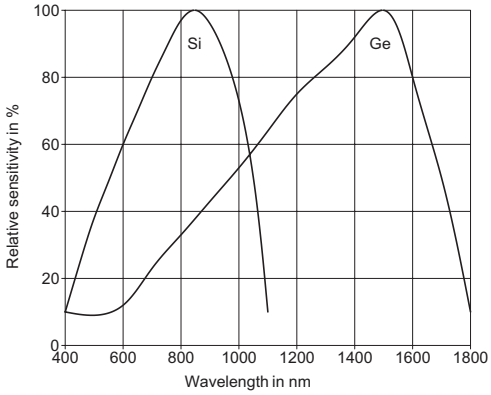

Fig. 14: Fig. 14: Relative sensitivity for Si and Ge photodetector

To achieve absorption of a photon at all its energy has to fit into the band structure of the material under consideration. From the condition

$$E_{ph} = \hbar\omega = h\nu = \frac{hc}{\lambda} \geq E_G$$

one recognises that for large wavelengths the energy of the photon may no more be sufficient „ to lift“ the electron in a way that it passes the band gap. For smaller wavelengths one has to respect that the conduction band and also the valence band have upper edges which is followed by a band gap. Photon energies which pass the upper limit of the conduction band can no more be absorbed. The wavelength of the applied light source decides which detector material is to be used. For wavelengths above 1 µm up to 1.5 µm Germanium is recommended. Underneath these values Silicon detectors are used. In the present experiment a laser diode of 810 nm wavelength is applied. Therefore a silicon detector is used.

To get a high quantum efficiency not a PN but a PIN detector has been chosen.

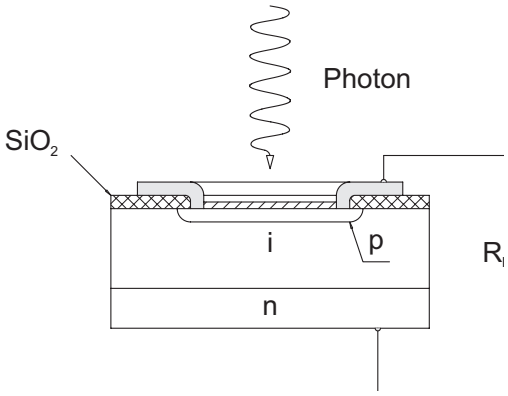

Fig. 15: Fig. 15: Construction of a PIN detector

Contrary to a detector with a simple pn-layer this type of detector has an intrinsic conducting layer inserted in between the p- and n-layer. Therefore the name PIN-diode. The reason for this is to enlarge the barrier layer which increases the probability of absorption of a photon and the generation of a current impulse, e.g. the quantum efficiency. The quantum efficiency for such an arrangement is:

$$\eta = (1-R)\left(1-e^{-\alpha d}\right)e^{-\alpha d_p}$$

R is the Fresnel reflection at the Si or Ge surface which is hit by the photons, a is the coefficient of absorption, d the thickness of the intrinsic zone and d_p the thickness of the p-layer. By attachment of a reflex reducing layer on the upper side of the p-layer R can get a value of less than 1%. Since the term αd_p is anyhow <<1, the thickness of the intrinsic layer should be chosen as large as possible. The consequence of this is that the drift time rises and the limiting frequency of the detector is reduced.
In so far a compromise between high quantum efficiency and high limiting frequency has to be made. In this experiment a PIN-Si-photo diode, type BPX61 is used. It has the following characteristic values:

Quantum efficiency η at 850 nm	90 %
Rising time 10%-90% at R_L = 50Ω and U_d=10V	1.7 ns
Capacity C_j at U_d =	
0 V	73 pF
1 V	38 pF
10 V	15 pF
dark current i_d at U_d = 10V	2 nA
Photosensitivity at U_d = 5V	70 nA/lx

We have now gathered all the necessary facts in order to understand the functioning of laser distance measurement devices. The experimental description follows after understanding the basics of OTDR.

2.6 Basics of OTDR

Any new foundations to elaborate on the working of the Optical Time Domain Reflectometer are really not required. The essential difference from the range finder is that instead of air, we use here glass fibre.
The measurement task is to identify and localise imperfections in the fibre. They can be, as an example in extreme cases, due to fibre cracks, defective fibre connector or inadmissible fibre bending. The OTDR not only permits us to de-

tect back reflections but is also able to measure transmission losses of the fibre. This is due to the fact that the production of optical fibres is not a perfect process. Micro-structures which are more or less distributed homogeneously, exist in every fibre and are a result of the manufacturing process. This is understandable when one is aware that glass fibres are drawn out of glass cylinders and therefore cannot be cooled down slowly as is the case in the manufacture of optical glass. In the case of the fibre, light which impinges on these micro-structures disperses in a manner such that the scattered light reaches back to the entrance of the fibre.

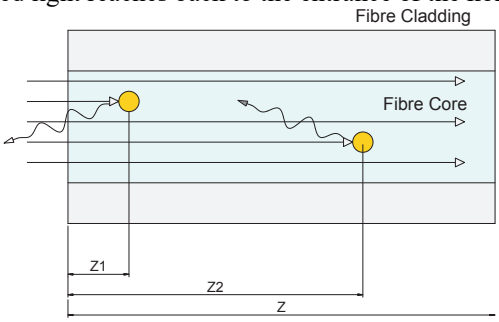

Fig. 16: Scattering centres in the fibre core

The above figure represents the situation in a simple manner. As the light wave hits on a scattering centre, the form and the dispersion of the scattered light depends on the ratio between the wavelength of the light and the size of the scattering centre. Because the wavelength is smaller in comparison to the scattering centre, one refers to it Mie - Scattering, in case however the wavelength is extremely small it is represented as Rayleigh-Scattering.
In such a case of appropriate ratio in a glass fibre, the results are represented in Fig. 17.

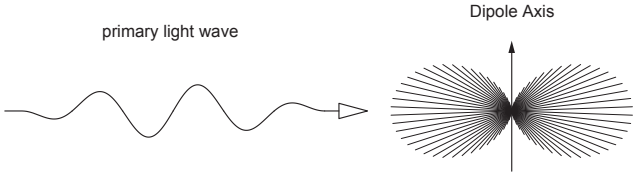

Fig. 17: Rayleigh-Scattering

The scattering centre whose diameter d <<λ, is considered a Hertz's dipole. Due to the impact of the electrical field (primary light wave) the dipole starts to oscillate which again is radiated from the dipole. With this, the direction of the beam is towards the dipole axis and results in a $\sin^2\upsilon$ distribution, where υ is the angle with respect to the dipole axis. The primary radiation has its maximum value for $\upsilon = \pm 90°$. The produced secondary radiation has the same wavelength as the primary wavelength, however in different directions. Consequently, such type of a scattering centre of the primary wave energy is extracted and results in the attenuation of the primary field. The main reasons for the formation of a scattering centre are varied. The scattered radiation which comes into being through the interaction of atoms and molecules respectively is unavoidable. In glass fibres more aspects are noticed because glass is a amorphous body which shows the remains of the crystal structure in a very limited zone. The structure which surrounds the centre is a disordered/ random structure. The crystal irregularities are small in comparison to the wavelength and therefore exhibiting the Rayleigh scattering behaviour. The refractive index of the irregularities differentiate themselves from the medium refractive index of the surrounded random structure, because of which the light from these zones is scattered. Depending on whether in the glass used, still further addition which are never homogeneous and completely solved, it comes to further variations of the refractive index, which represents again scattering centres:

The attenuation which a light wave experiences because of its scattering can be formulated like an absorption:

$$I(z) = I_0 \cdot e^{-\alpha_R \cdot z}$$

Whereby the attenuation coefficient α_R is given as:

$$\alpha = \frac{4\pi^3}{3 \cdot \lambda^4} \cdot \overline{\left(n^2 - \overline{n^2}\right)^2} \cdot d_C^3$$

Thereby is

$$\overline{\left(n^2 - \overline{n^2}\right)^2}$$

the mean variation square of the difference of the refractive index of the fibre to that of the irregularities. The term d^3_C describes the volume of such type of irregularities. An interesting aspect is the dependency of the attenuation of the fourth power of wave length. For the practical estimation of the attenuation in dB, one uses the equation:

$$\alpha(\lambda) = \alpha_{1\mu m} \cdot \frac{1}{\lambda^4} \approx 0{,}63 \cdot \frac{1}{\lambda^4} \left[dB / km\right]$$

With that, the attenuation of the pure silica glass by the wave length of 1 µm is $\alpha_{1\mu.}$ The numerical value of the wave length must be given in µm. With a wavelength of 810 nm for example, one expects an attenuation of 1.46 dB/km.
The attenuation through absorption, and therefore through the excitation of electrons takes place with glasses only in the UV wavelength area and by wavelengths from 2 µm through the absorption of IR molecules in the glass. This kind of attenuation in comparison to attenuation through scattering can be neglected here.
The undesirable yet unavoidable occurrence of the scattering in the fibres is therefore essentially responsible for the attenuation in fibres. However, it must be ensured in the production process that unavoidable scattering remains at the lower limit. But even in practical installation, the attenuation can be negatively influenced because of outside influences. Therefore, a reliable method is required to be able to monitor the attenuation during the finishing process as well as for existing glass fibre networks. Here one utilises the scattered light itself which anyway is dampened. Due to the fact that the radiating feature of the scattered light also reaches back at the entrance, one can detect it there and observe its intensity course with respect to the start of a light pulse. The transitory change of the scattered light gives then the information over the attenuation of the fibre. For understanding this we go back once again to Fig. 16.
The light which is scattered at the point z_2 has a longer travel path to the fibre entrance as that one which has arisen at point z_1. Due to the loss in the fibres, the scattered light from position z_2 is weakened more than the one from the position z_1. Due to this it reaches the detector later due to the different transit time. One sends only a pulse with time duration t_p into the Fibre. In this manner one gets an answer as shown in Fig. 18.

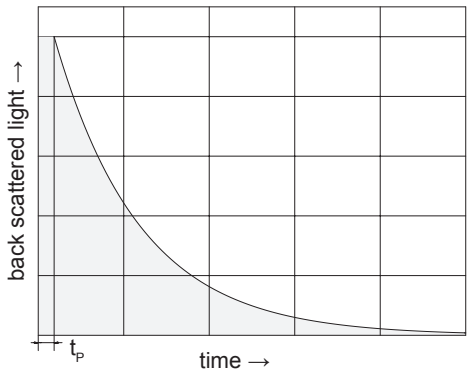

Fig. 18: Transitory result of the scattered light from the fibres.

One scales the output of the back scattered light logarithmically. In this way a straight line comes up comprising of the attenuation. In practice this does not result in a smoothened curve like in Fig. 18. However with linear regression, meaningful values can be achieved.

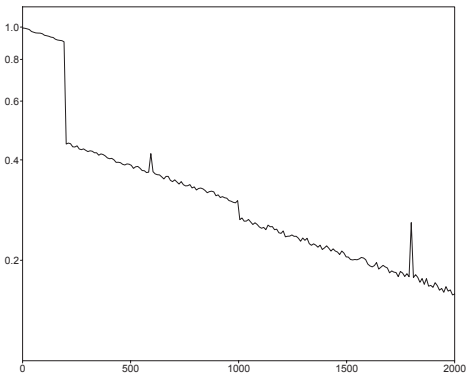

Fig. 19: Example

The above example depicts such a type of logarithmically representation. Near to the attenuation losses, one observes a series of other effects. One of them is the local loss and the other are reflections at irregularities.

So far for the motivation of the measuring task. How the light comes into the fibres and is transported has been elaborated in the next paragraph.

There is hardly any book in optics which does not contain the experiment of Colladan (1861) on total reflection of light. Most of us may have enjoyed it during the basic physics course.

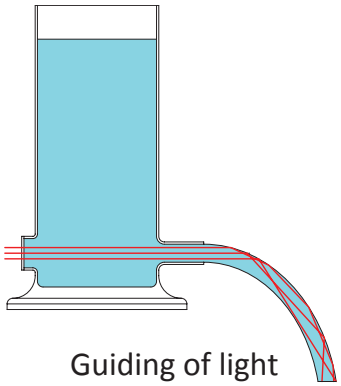

Fig. 20: Colladan's (1861) experiment for the demonstration of the total reflection of light

An intensive light beam is introduced into the axis of an out flowing water jet. Because of repeated total reflections the light can not leave the jet and it is forced to follow the water jet. It is expected that the jet remains completely darken unless the surface contains small disturbances. This leads to a certain loss of light and it appears illuminated all along its way. Effects of light created in this way are also known as „Fontaines lumineuses". They please generally the onlookers of water games. This historical experiment already shows the physical phenomena which are basic in fibre optics. The difference of this light conductor to modern fibres is the dimension which for a fibre is in the order of magnitude of the wavelength of light. If we designate the diameter of a light guide with d we can stat

„Fontaines lumineuses"	$d \gg \lambda$
Multimode fibres	$d > \lambda$
Monomode fibres	$d \approx \lambda$

For the fibres manufactured these days this leads to further effects which can not be described exclusively by total reflection. Their understanding is of special importance for optical communication technology. In the following we will deduce these effects based on Maxwell's equations. For the work in fibre optics it is not compulsory to know this formalism. It is sufficient to familiarise oneself with the results.

2.7 Fibres as light wave conductors

Glass fibres as wave conductors have a circular cross section. They consist of a core of refractive index n_k. The core is surrounded by a glass cladding of refractive index n_m slightly lower than n_k. Generally the refractive index of the core as well as the refractive index of the cladding are considered homogeneously distributed. Between core and cladding there is the boundary as described in the previous chapter. The final direction of the beam is defined by the angle Θ_e under which the beam enters the fibre. Unintended but not always avoidable radiation and cladding waves are generated in this way. For reasons of mechanical protection and absorption of the radiation waves the fibre is surrounded by a protective layer.

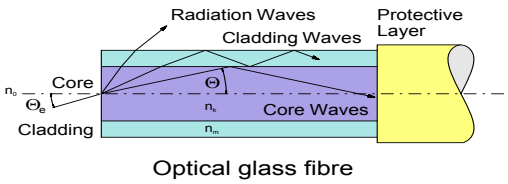

Fig. 21: Step index fibre

Fig. 21 reveals some basic facts which can be seen without having solved Maxwell's equations. Taking off from geometrical considerations we can state that there must be a limiting angle Θc for total reflection at the boundary between cladding and core.

$$\cos(\Theta_c) = \frac{n_m}{n_k} \qquad \textbf{(8)}$$

For the angle of incidence of the fibre we use the law of refraction:

$$\frac{\sin(\Theta_{ec})}{\sin(\Theta_c)} = \frac{n_k}{n_0}$$

and obtain:

$$\Theta_{ec} = \arcsin\left(\frac{n_k}{n_0} \cdot \sin\Theta_c\right)$$

Using equation (8) and with $n_o = 1$ for air we finally get:

$$\Theta_{ec} = \arcsin(\sqrt{n_k^2 - n_m^2})$$

The limiting angle Θ_{ec} represents half the opening angle of a cone. All beams entering within this cone will be guided in the core by total reflection. As usual in optics here, too, we can define a numerical aperture A:

$$A = \sin\Theta_{ec} = \sqrt{n_k^2 - n_m^2} \qquad (9)$$

Depending under which angle the beams enter the cylindrical core through the cone they propagate screw like or helix like. This becomes evident if we project the beam displacements onto the XY-plane of the fibre. The direction along the fibre is considered as the direction of the z-axis. A periodical pattern is recognised. It can be interpreted as standing waves in the XY-plane. In this context the standing waves are called oscillating modes or simply modes. Since these modes are built up in the XY-plane, e.g. perpendicularly to the z-axis, they are also called transversal modes. Modes built up along the z-axis are called longitudinal modes. For a deeper understanding of the mode generation and their properties we are now going to solve the Maxwell equations under respect of the fibre boundary conditions.

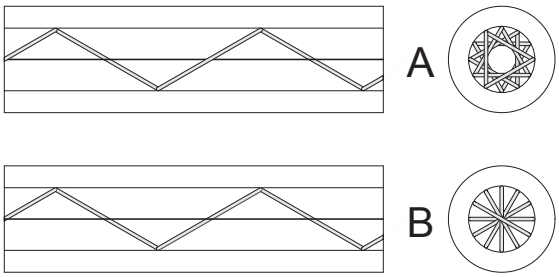

Fig. 22: Helix (A) and Meridian rays (B)

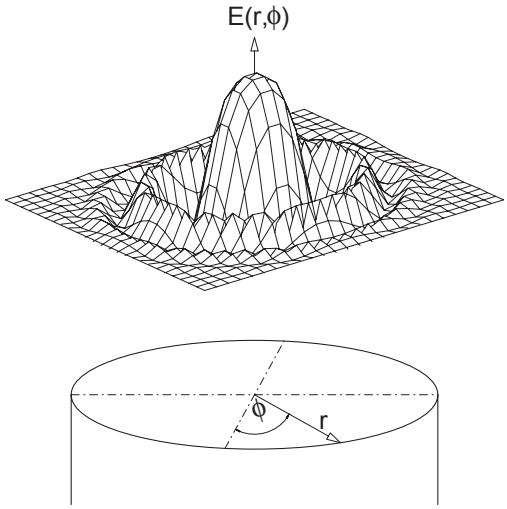

Fig. 23: Fig. 23: Solution of Bessel-function for p=0

Fig. 23 presents the solution for p=0. Because of the f dependence the rotational symmetry is lifted for solutions with p≠0. Already now we see how the electric field will establish within the core. It also gets clear that the radius of the fibre will be decisive for the order p of the modes. In the radial direction of the fibre we observe a main maximum at r = 0 and further aside maxima or minima which are also called nodes. The number of nodes, which will later be characterised by the counter index q, is determined by the diameter of the fibre as well as by the solution of the wave equation within the cladding. After having chosen a suitable cylindrical function for the solution within the cladding, it has to be ensured that it matches the continuity conditions for the electric and magnetic field at the boundary between core and cladding. This leads to the complete solution. For the final solution of the problem one uses modified Hankle functions and the approximation of weakly guiding fibres. Still, because of technical reasons it is not possible to choose the refractive index of the core much larger than the refractive index of the cladding. Since core and cladding are in close contact glasses of similar temperature coefficient can only be used. The consequence of this is the small difference in refractive index. For ordinary fibres it is

$$\frac{n_k - n_m}{n_k} \approx 2 \cdot 10^{-3},$$

where the refractive index n_k of the core is equal to 1.465.
One important result of the calculations gives the dimensioning rule for optical fibres:

$$1.5 < \frac{2\pi}{\lambda} \cdot r \cdot \sqrt{n_k^2 - n_m^2} \le 2.405$$

For a given wavelength l and index of refraction of the core and cladding one can calculate the necessary radius of the core in order to efficiently transport mono mode light via the fibre.
If we are using as for example the light of an HeNe-Laser at a wavelength of 633 nm we obtain as upper limit for the core radius:

$$r < 2.405 \cdot \frac{633 \cdot 10^{-9}}{2\pi\sqrt{(1.465)^2 - (1.462)^2}} = 2.6\mu m$$

According to this the diameter of the fibre core should be less than 5.2 µm in order to transport mono mode light. Within the frame of this project we are not interested in signal transmission rather than in testing fibres. But for this purpose we have to know how to couple the light of the used laser diode efficiently to the to be tested fibre.

2.8 Coupling of light to fibre

We are facing the problem to couple a beam of light to a fibre, respectively to introduce it into a fibre, the diameter of which is in the order of magnitude of 4-10 µm and in so far comparable to the wavelength of light. To get a sufficient high excitation of the fundamental mode of the fibre, the beam of the light source has to be focused to a diameter of this order of magnitude. Under these circumstances the laws of geometrical optics fail because they anticipate parallel light beams or plane light waves which in reality exist only in approximation.
To get a maximum of power into the fibre a coupling optic of focal distance f is required assuring the coupling of a Gaussian beam into a weak guiding step index fibre in the LP_{01} fundamental mode.

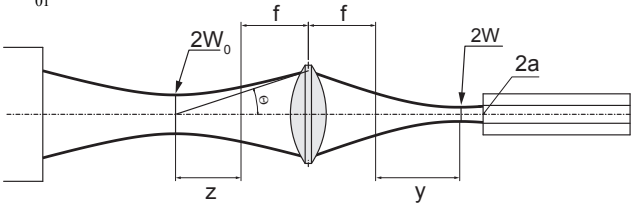

Fig. 24: For the calculation of the coupling optics

Radius at the waist

$$w = \frac{w_0 \cdot f \cdot \theta \cdot}{\sqrt{w_0^2 + \theta^2 \cdot z^2}}$$

Location of the beam waist

$$y = \frac{z \cdot f^2}{z^2 + \left(\frac{w_0}{\theta}\right)^2}$$

Example: The beam of a HeNe laser of 0.5 mm diameter and of 1.5 mrad divergence is to focus by means of a lens. The focal distance is 50 mm and the lens is at a distance of 2 m from the laser. We find:

$$w = \frac{0,5 \cdot 10^{-3} \cdot 0,05 \cdot 1,5 \cdot 10^{-3}}{\sqrt{0,25 \cdot 10^{-6} + 2,25 \cdot 10^{-6} \cdot (2 - 0,05)^2}} = 12,6 \mu m$$

$$y = \frac{(2 - 0,05) \cdot 2,5 \cdot 10^{-6}}{(2 - 0,05)^2 + \left(\frac{0,5}{1,5}\right)^2} = 1,25 \mu m$$

For this example the position y of the waist coincides with the focus in good approximation and the radius of the waist is here 12.6 µm. To get the fibre under consideration adapted in an optimal way the focal distance f has to be chosen in a way that the radius of the beam is equal to the radius of the core. When laser diodes are used the preparation of the beam becomes more complicated.

After having dealt with glass fibres as well as the introduction of light sources, we turn to the construction of the OTDR.

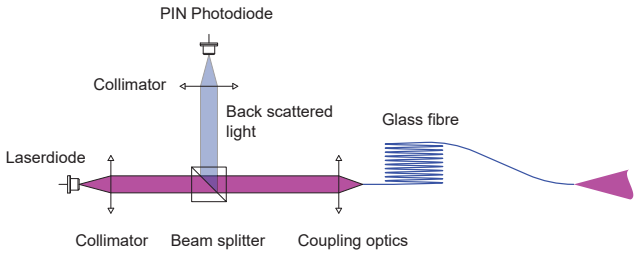

Fig. 25: Fig. 25: Set-up of an OTDR

The radiation of the laser diodes is collimated and passes a polarized beam splitter. As the laser light is well polarized, it reaches the coupling optics with low losses. There it is launched into the fibre.

One still cannot achieve to launch the complete light into the fibre. Unavoidable back reflections arise through Fresnel-Reflections. Also one fails to achieve a perfect match of the beam diameter to the fibre core diameter. Due to this reasons a relative amount of back reflection of the laser light arises on the entrance surface of the Fibre which is directed back to the polarized beam splitter. Depending on the polarization of the light which has been reflected back, a part reaches the detector and another the laser diode. The light which falls onto the photodetector is used as a initial signal for measurement.

As elaborated, a part of the reflected and scattered light from inside the fibre leaves the fibre entrance due to disturbances. This light has mainly another polarization state than the incoming. The reason for this can be found in the interpretation of the Rayleigh - scattering and polarization through reflection.(Fresnel equations)

2.9 Selection of a suitable laser

For both types of measurements, LIDAR and OTDR, different requirements are addressed to the laser light source. However, we also have common characteristics. The wavelength of the laser should be close to the maximum sensitivity so that reasonably fast photodetector can be used. This is well accomplished with 905 nm laser diode in connection with Si PIN photodiodes.

Laser diodes with this wavelength are available in large numbers with differently varying outputs. In addition, they should be able to emit short pulses. One can differentiate between two types of laser diodes, ones that are only for pulsed operation and the others that can work in a continuos as well as in the pulse mode. Laser diodes which work only in the pulsed mode posses a very high maximum output up to a few 100 Watts. Their wavelength is close to 900 nm. This enables their use in the measurement of large distances without requiring a triple reflector. As the emission profile does not correspond to the Gaussian fundamental mode, good divergence values are not obtained. Continuously working laser diodes can in general work very well in pulsed operation. In addition, the injection current can be modulated. Even though the output power is not as high as in the pulsed laser diodes, these laser diodes are available with TEM_{00} . Furthermore, they also permit a full control over the duty cycle. This is limited to approximately 1-5% in the case of pulsed diodes. This enables the laser pulse signals given out to be definite and thus provide improvement in the reduction of interference in the measuring method.

Meanwhile the characteristics of pulse diode laser has been significantly improved so that within this experiment such a diode laser is used.

3.0 Description of the components

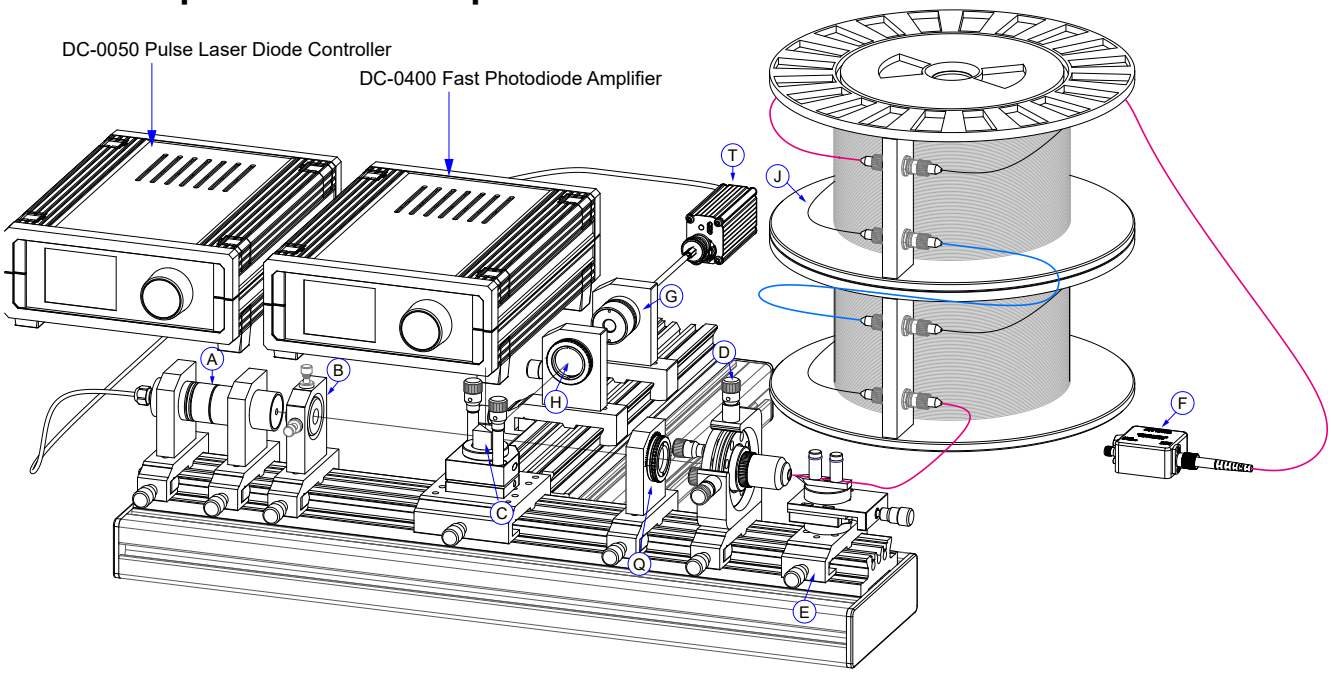

Fig. 26: Experimental set-up of the OTDR

3.1 Module A Laser Diode

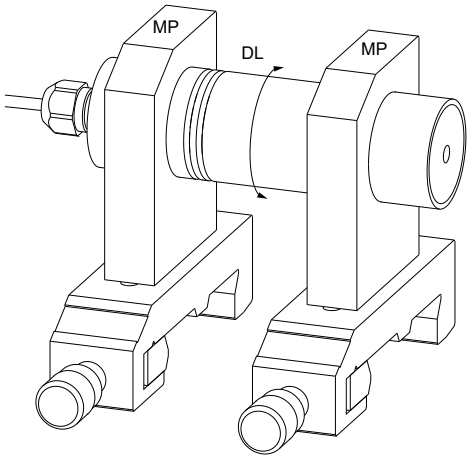

Fig. 27: Module A Laser diode

This module consists of two mounting plates (MP) in which the laser diode (DL) is mounted and can be rotated around its optical axis to set the direction of polarisation. Very fast electronic control is integrated in the laser head. The laser diode utilised is a pulsed laser diode with a maximum output energy of 5 µJ with a wavelength of 905 [± 10 nm]. The laser diode is connected with the control unit “DC-0050 Pulsed laser diode controller MK1”.

3.2 Diode Laser Controller DC-0050

Fig. 28: Controller DC-0050 for pulsed and cw laser diodes

The laser diode module is connected via the 15 pin HD SubD jacket (LED/LD). The controller reads the EEPROM of the laser diode and sets the required parameter accordingly. The MK1 is powered by an external 12V/ 1.5 A wall plug supply.. A USB bus allows the connection to a computer for remote control. Furthermore, firmware updates can be applied sim ply by using the same USB bus.

The MK1 provides an internal modulator which allows the periodic on/off switch of the diode laser. A buffered synchronisation signal is available via the BNC jacket (MODULATOR).

This controller is designed to operate the pulsed laser diode The fully digital operating device provides the charging voltage for the ignition capacitor of the pulsed laser diode as well as the trigger signal to ignite the laser pulse. By means of a one knob interaction all parameters can be set and displayed.

Charging Voltage: 10 ... 20 V in steps of 1 V
Repetition rate: 1 ... 2000 Hz in steps of 1 Hz
Pulse width control: 40 ... 150 ns
Operating Voltage: 12 V DC
Inputs: Diode laser connection
Outputs: Trigger as TTL signal via BNC jacket

+Further detailed specifications are given in the following section of the operation software.

When the external 12 V is applied, the controller starts displaying the screen as shown in the figure below.

Theory

3.2.1 Laser Safety

The first interactive screen requires the log in to the device since due to laser safety regulations unauthorized operation must be prevented. In general, this is accomplished by using a mechanical key switch. However, this microprocessor operated device provides a better protection by re-questing the entry of a PIN.

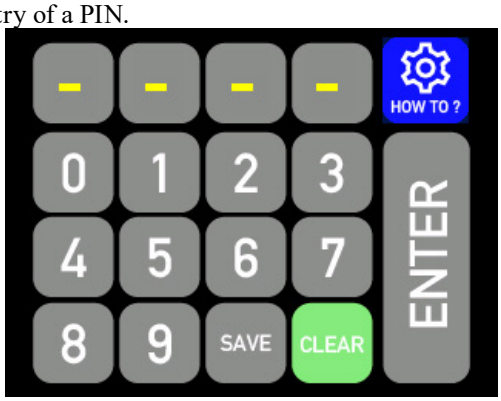

After entering the proper key, the next screen is displayed, and the system is ready for operation.

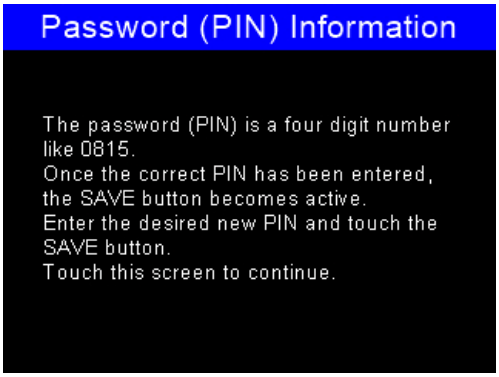

Touching the “HOW TO” button explains how to change the password.

In case that no laser has been connected, the controller shows the screen as shown above.

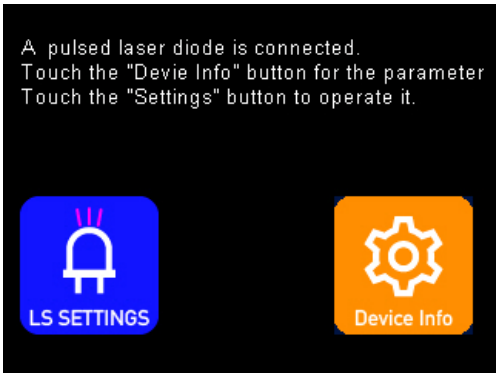

However, ff the pulse laser diode is properly connected the settings and info screen appears.
Touching the “Device Info” button changes to the info screen:

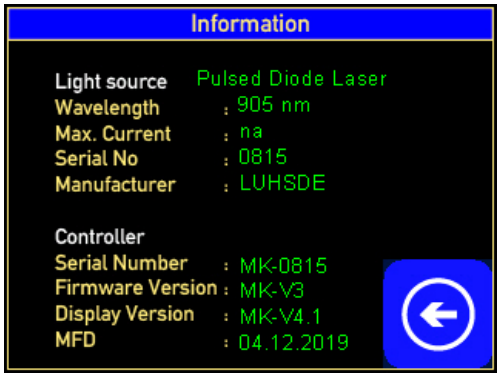

Touching the “LS SETTINGS” switches to the settings screen as shown below:

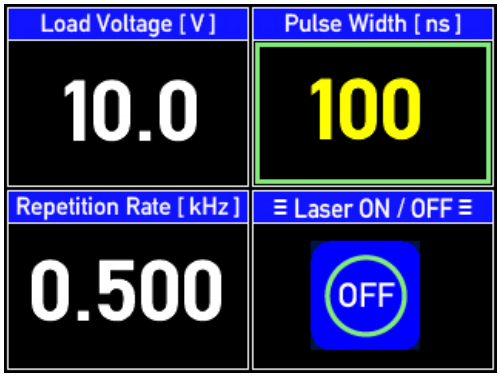

Touching the display field activates it and with the rotating digital knob the desired value can be set.

3.3 Module B Collimating Optics

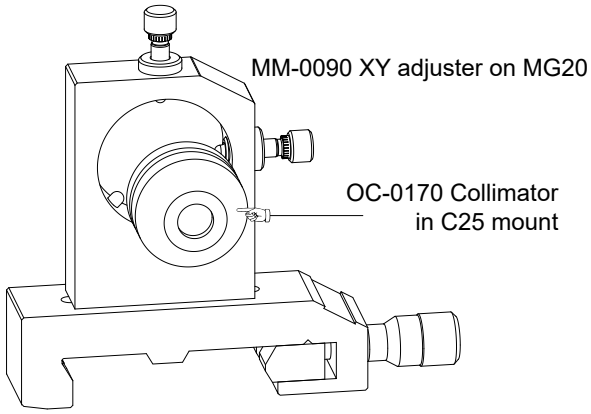

Fig. 29: Module B Collimating optics

A high precision aspheric glass lens is mounted into a click holder (A) which is inserted into the XY adjuster. With the fine pitch screws the collimator (OC-0170) can be adjusted accordingly. The glass lens has a focal length of 4.6 mm, the numerical aperture is 0.53 and the clear opening is 4,9 mm. In addition, the lens has an antireflex coating in a spectral range of 700 - 920 nm with a residual reflection of < 0.5 %.

3.4 Module C Beam Splitter

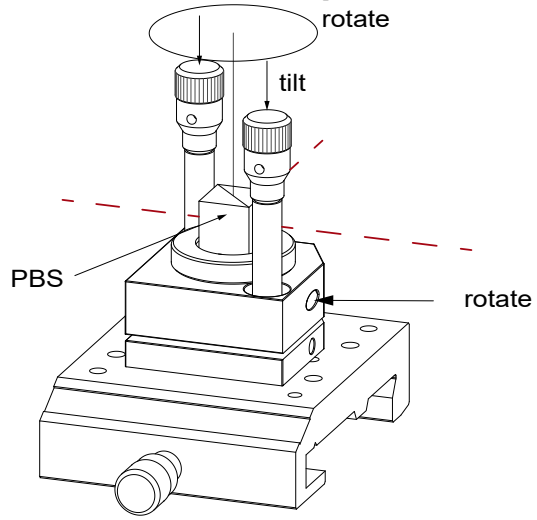

Fig. 30: Module C beam splitter

The adjustable prism holder is installed on a tee piece carrier. With the fine pitch screws, the polarised beam splitter can be orthogonal tilted. In addition, the cube can be rotated around its vertical axis. For this, Allan keys (1.5 and 2 mm) are provided.

3.5 Module Q rotatable λ/2 plate

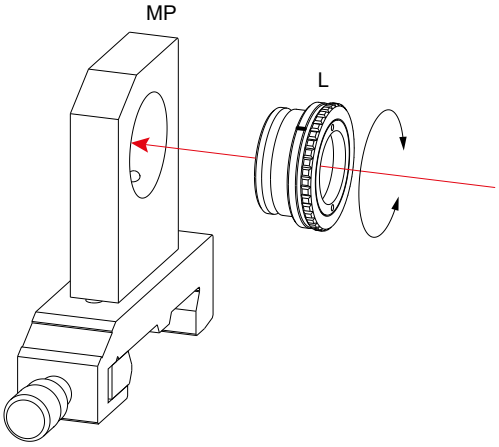

Fig. 31: Module Q rotatable λ/2 plate

Together with the polarised beam splitter Module C, this element forms an optical diode which suppresses a considerable part of the undesired returning reflected light. The rotation of the plate optimise the effect.

3.6 Module D Coupling Optics

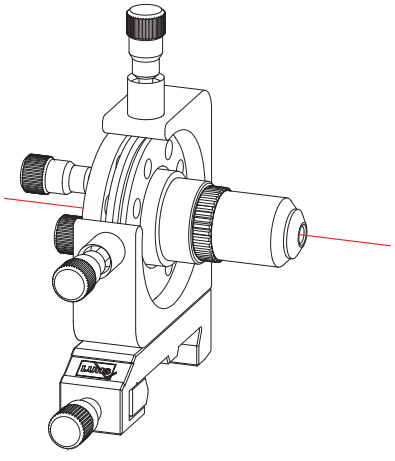

Fig. 32: Module D Coupling Optics

Basically the same arrangement as module B but with a fine adjustment holder with four axis XY, θ and ϕ and an objective of smaller focal distance to focus the collimated laser diode radiation in such a way that an effective coupling to the fibre is ensured. Purposely a beam shaping of the laser diode radiation has been omitted to simplify the entrance into the experiment.

3.7 Module E Fibre holder with translation stage

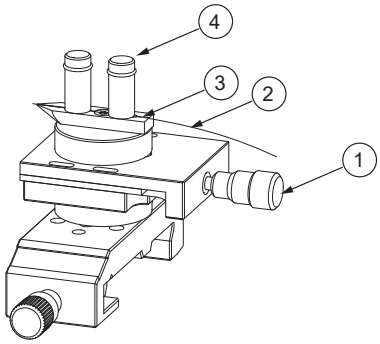

Fig. 33: Module E Fibre holder with translation stage

The prepared glass fibre (2) is inserted into the groove of the holder (3) and is fixed in its position by means of two magnets (4). The stage (1) permits the fine displacement in the direction of the optical axis for the optimization of the coupling.

3.8 Module H imaging optics

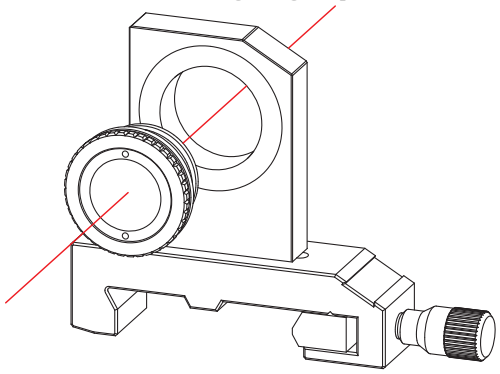

Fig. 34: Module H imaging optics

A lens with a focal length of 60 mm is used to focus scattered and reflected light on the sensitive area of the detector of the Module G.

3.9 Module G SiPIN detector

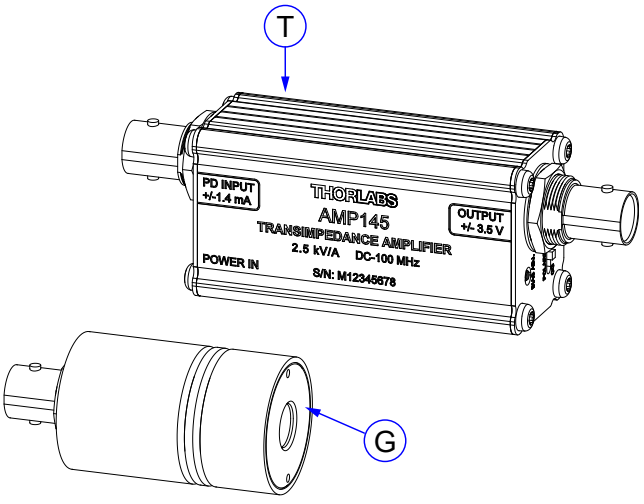

Fig. 35: Module G SiPIN detector

To achieve a highest possible cut off frequency (0.4 GHz) a Si

PIN photodiode (G) with a corresponding fast trans impedance preamplifier (T) is used. The transimpedance amplifier has an in-line box design with two female BNC connectors and is intended to be used between two BNC cables. The device is powered through a Micro-B USB port using the included 5 V, 2 A power supply or any other available USB port. The internal electronics of the amplifier regulate the power to the amplification circuitry, isolating the device's performance from electrical noise that may be inherent to the power source.

At the OUTPUT end of the amplifier, a small switch allows users to choose the polarity: AG (anode grounding) or CG (cathode grounding). The bias voltage can be adjusted from 1.2 V up to 15 V with the BIAS ADJ screw on the OUTPUT end.

Caution: The outer conductor at the INPUT BNC connector carries potential and shall not be grounded. Attach only devices to the INPUT BNC of the AMP145 that are not attached to ground or else it will short circuit the AMP145 and may break the device.

The Si PIN photodiode (BPX61) has a large sensitive area (2.65 x 2.65 mm) and a junction capacity of 15 pF at a reverse voltage of 9 V. The pre-amplified signal is available at the BNC coax receptacle and is connected via an RG-174 cable to the DC-0400 Amplifier. The photodetector module is placed into the mounting plate (MP) where it is kept in position by three spring loaded steel balls.

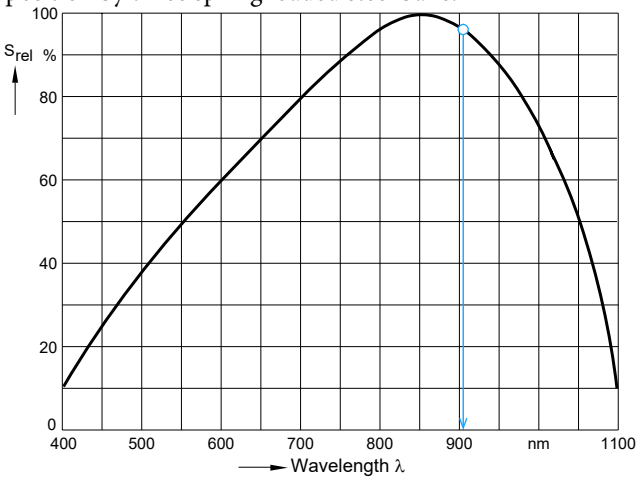

Fig. 36: Spectral sensitivity curve of the BPX61 photodiode

At the emission wavelength of the pulsed diode laser of 905 nm the sensitivity of the BPX61 photodiode is almost maximal.

Parameter	Symbol	Value
Rise and fall time of the photo current at: R_L=50 Ω, V_R=5V, λ=850 nm and I_P=800 µA	t_r, t_f	20 ns
Forward voltage I_F = 100 mA, E = 0	V_F	1.3 V
Capacitance at V_R = 0, f = 1 MHz	C_O	72 pF
Wavelength of max. sensitivity	λ_{Smax}	850 nm
Spectral sensitivity S~10% of S_{max}	λ	1100
Dimensions of radiant sensitive area	$L \times W$	7 mm²
Dark current, V_R = 10 V	I_R	≤30 nA
Spectral sensitivity, λ = 850nm	$S(\lambda)$	0.62 A/W

Table 1: Basic parameters of Si PIN photodiode BPX61

3.10 Photodetector (F) with FC fibre receptacle

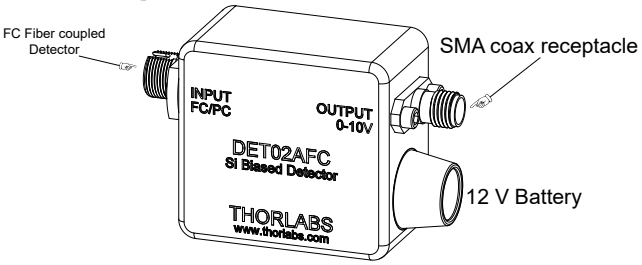

Fig. 37: Photodetector (F) with FC fibre receptacle

The DET02AFC is a ready-to-use, high-speed Si photodetector for use with FC/PC connectorized fiber optic cables in visible optical systems. The unit comes with an FC/PC bulkhead connector, detector, and 12 V bias battery enclosed in a compact aluminum housing. The FC/PC connector provides easy coupling to fiber-based light sources. The output uses an SMA jack to minimize size and maximize frequency response. The maximum bandwidth is 1 GHz and will operate over the spectral range of 400 – 1100 nm. It used to connect the output of a fibre drum directly to the photodetector. With the provided SMA/BNC cable the detector is connected to an oscilloscope, which input impedanve needs to set to 50 Ohms.

3.11 DC-0400 Hi speed photodetector amplifier

Fig. 38: Front of DC-0400 Hi speed photodetector amplifier

The DC-0400 contains a micro processor controlled hi speed amplifier with an adjustable gain of 20 to 52 dB (10 times to 398 times). The input is set to either DC or AC coupled.

Fig. 39: Rear view of the DC-0400 Hi speed photodetector amplifier

The DC-0400 is operated by an external wall plug power supply which is connected to the 12V DC input. The USB bus is used to update the firmware. The 9 pin Sub-D connector of the photodiode is connected to the "PHOTODIODE" receptacle with the provided SMA/SMA cable. The signal of the photodetector is connected to the SMA receptacle "IN". The line impedance is 50 Ohms. The amplified signal is available at the SMA connector "OUT". With the provided SMA/BNC cable the amplified signal can be connected to an oscilloscope.

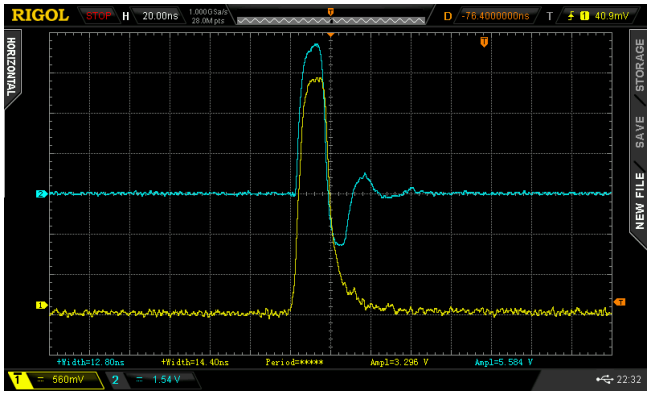

Fig. 40: Test measurement with a 20 ns short pulse laser. It should be noted that the rise time of the oscilloscope is 5 ns.

The upper blue track shows the electronic trigger signal of the laser diode and the yellow one the amplified photodetector.

Fig. 41: Start screen

When the toggle switch on the rear of the DC-0400 is switched on, the start screen appears. Touching the screen brings up the main screen.

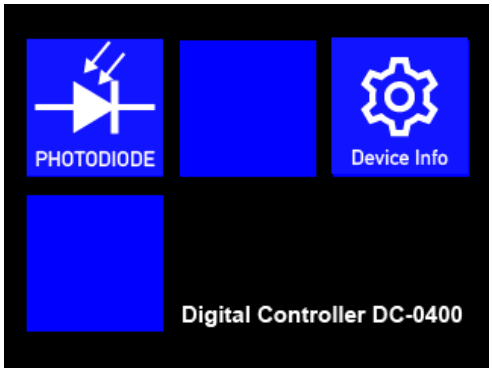

Fig. 42: Main screen

The main screen provides two buttons. The “PHOTODIODE” button changes to the amplifier screen and the “Device Info” button changes to the info screen.

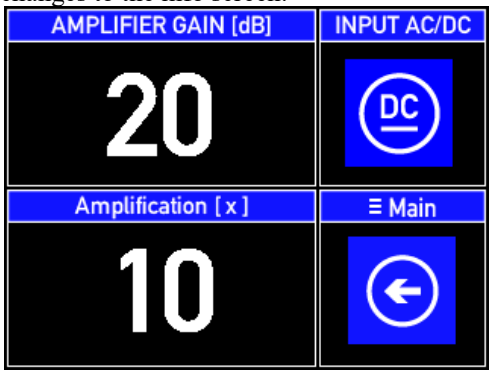

Fig. 43: Amplifier screen in DC mode

By turning the digital knob the value of the amplifier gain is set in a range from 20 to 52 dB related to an amplification factor from 10 to 358 times.

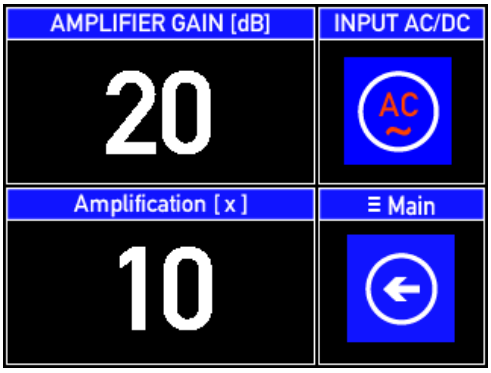

Fig. 44: Amplifier screen in AC mode

Touching the “INPU AC/DC” button toggles to AC. In this mode the amplifier is AC coupled.
Please note:

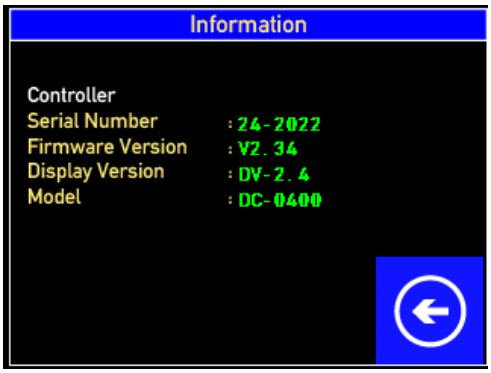

Fig. 45: Info screen

3.12 Module J 1000 m of multimode fibre

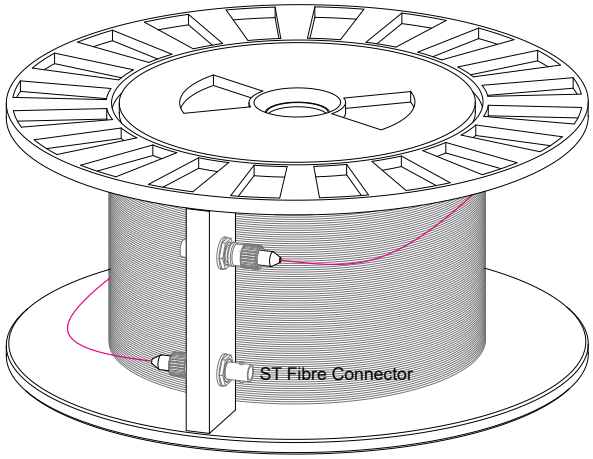

Fig. 46: Module J 1000 m of multimode fibre

A drum carries 1000 metres of a multimode fibre with a fibre core diameter of 50 µm and a cladding of 125 µm. The fibre ends are terminated by ST connectors which are connected to ST fibre panel jacks. The provided pigtailed fibre are bare on one side and terminated by an ST connector on the other end. Within the experiment the preparation of the fibres, like stripping and cleaving is trained. This is performed with the bare end of the fibre pigtails and does not effect the 1000 m long main fibre. Furthermore multiple fibre drums can be connected in series to study the effect of longer fibres. For the OTDR measurements a multimode fibre with a core

diameter of 50 mm is used. The exact length is given on the drum label. Commonly, these are approximately over 1,100 m.

3.13 Preparation of the pig tailed fibre cable

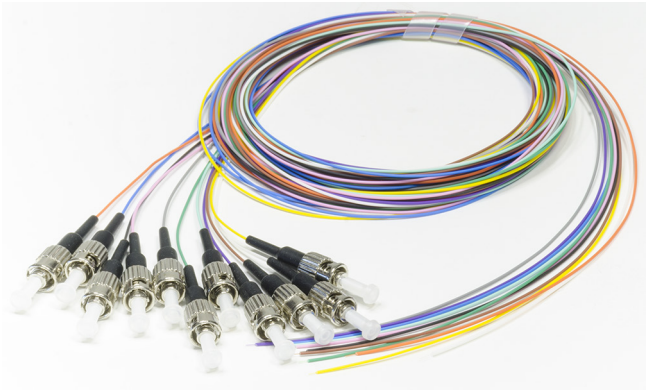

Fig. 47: Pig tailed fibre patch cable

Before the fibre can be used it has to be prepared in such a way that the bare fibre end surface is perpendicular to the core axis and of best optical quality. This is achieved by controlled breaking of the fibre using a one step fibre cleaver and breaker. Before this can be done the plastic buffer coating has to be removed, which is done by using so called Miller's pliers. It is a kind of cable stripper however for a thin cable of 0.9 mm. After the removal of the buffer plastic jacket, the plastic cover of the glass fibre (250 - 125 µm) is removed as well.

3.14 Miller's pliers

Fig. 48: Miller's pliers

The pliers must be adjusted that the closed pliers does not injure the cladding glass of the fibre when stripping the plastic buffer. The pliers are coming pre-adjusted and if necessary the fixing screw of the diameter set screw is loosened and the diameter set screw is aligned.
After both the plastic buffer has been stripped, the fibre is ready for cleaving and breaking.
For this purpose a cleaving and breaking tool is used.

3.15 Fibre Cleaver

Fig. 49: The fibre cleaver FC-6S.

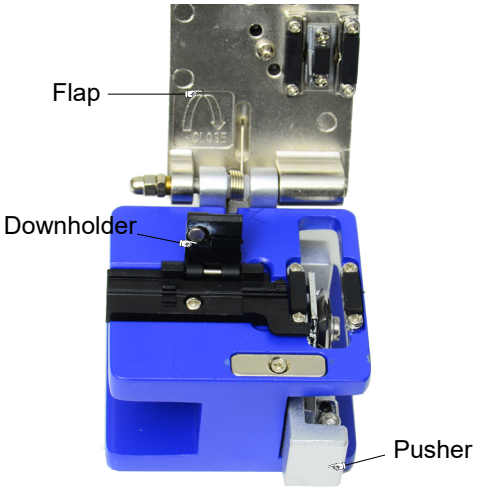

Fig. 50: Cleaver with opened flap

Before inserting the fibre, the down holder is lifted.

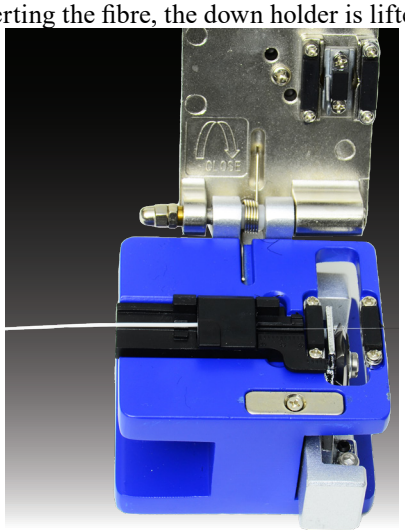

Fig. 51: Inserted fibre

The inserted fibre is clamped and held in position by the down holder. The length of the fibre is chosen such that 20-30 mm protrudes the housing.

Fig. 52: Scribing and breaking

The flap is closed and the pusher is pushed into the device where it remains until the flap is lifted again.

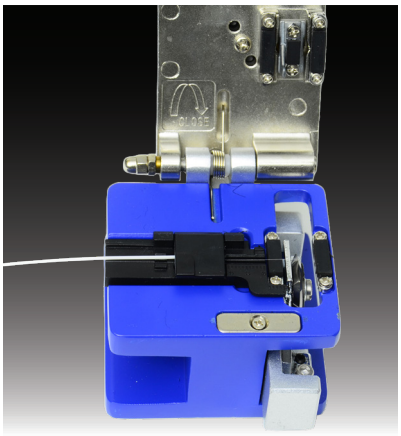

Fig. 53: Read cut fiber

After opening the flap, the pusher moves back into its initial position. Lift the down holder and take the fibre out.
Attention: Remove the residual splint of the fibre from the rubber clamp and deposit it into a fibre scrap can to avoid that these parts may enter and injure the human body.

4.0 Experiments

4.1 Characterising the pulse diode laser

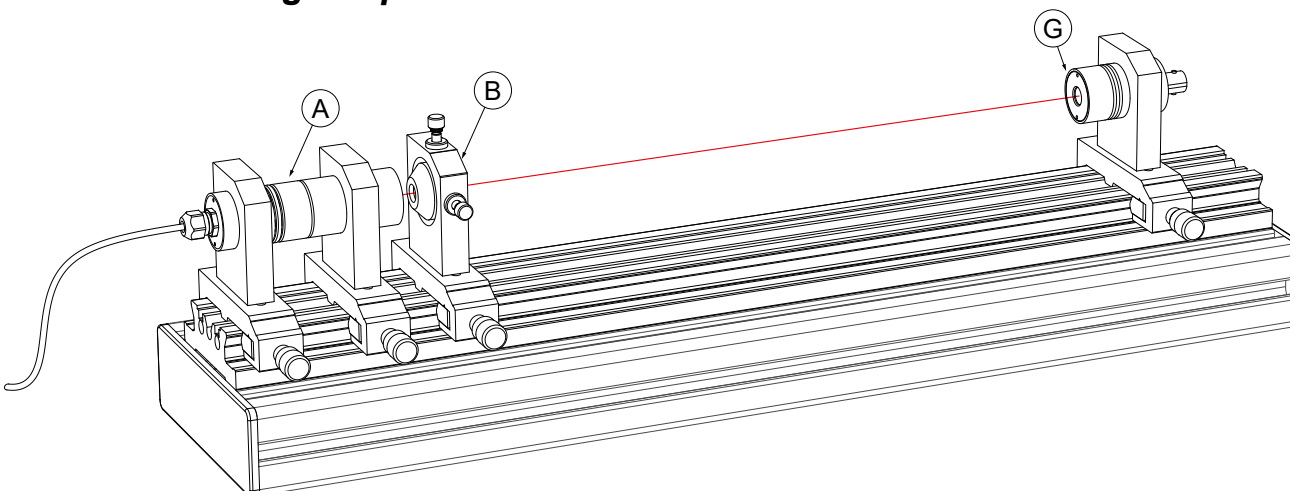

Fig. 54: First step in the set-up of the OTDR

The emitted radiation of the pulsed diode laser has a wavelength of 905 nm which is not visible to the human eye.

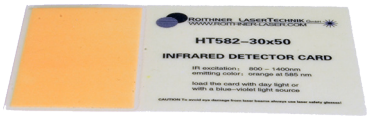

Fig. 55: Infrared detector card

The set-up starts with the collimation and alignment of the laser radiation of the diode laser (A) as shown in Fig. 54. The photodetector (G) is used as alignment target to the centre the beam to the mechanical axis. The infrared detector card is used to check the beam parallelism and location.

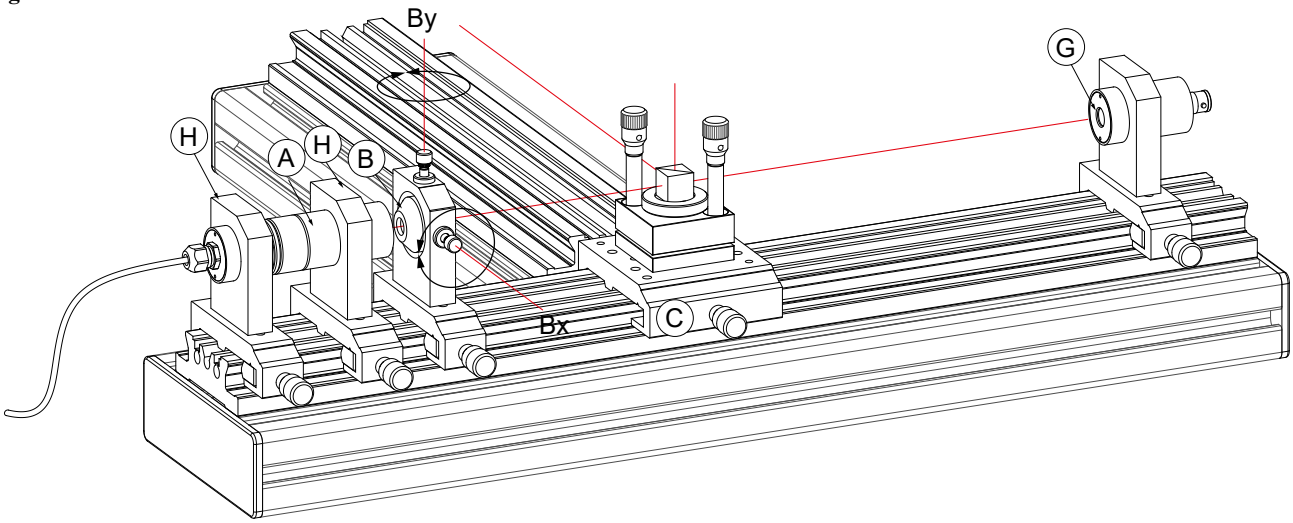

Fig. 56: Second step in the set-up of the OTDR

In a first task the properties of the pulsed diode laser are studied. For this purpose only the modules are shown in the Fig. 56 are required. The peak pulse is measured as a function of the load voltage and repetition rate using the photodetector G. G is connected via module T to an oscilloscope to monitor the signal. The laser diode's data can be used to determine the peak power.

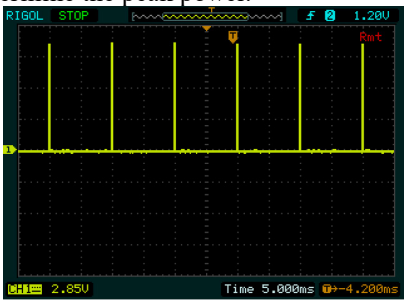

Fig. 57: Measuring the repetition rate

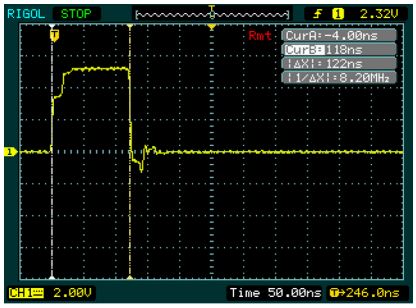

Fig. 58: Measuring the pulse width

The diode laser (A) can be rotated within the holder (H) and the polarisation recorded for different angle positions. For the OTDR measurements it is important that the diode laser is orientated in such a way that the maximum of intensity passes the polarising beam splitter (C).
In the next step, the coupling to fibre optics as well as the λ/4 plate is set onto the optical rail.

4.2 Step by step set-up of the OTDR

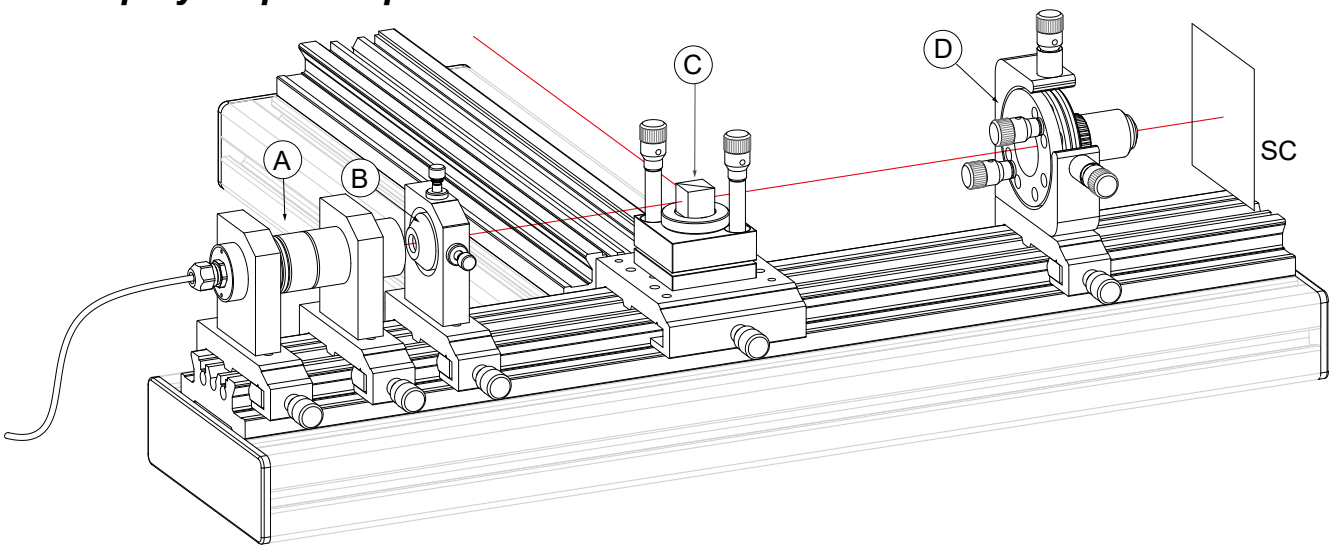

Fig. 59: Installation of the coupling optics

A focus should appear nearly close to the exit of the coupling optics. To check this with the provided infrared detector card with a moderately darkened room. Now slightly away from the focus, one still observes whether the laser beam passes through the microscope objective without hindrance. If not, then it is adjusted with B. The translation stage (E) should be set approximately in the middle of its travel range of 5 mm and is placed on the optical rail in such a way that the top of the fibre chuck is approximately 5 mm apart from the objective. Through lateral and top view one can see that the centre of the coupling optics (D) in X and Y direction coincides with the tip of the fibre chuck.

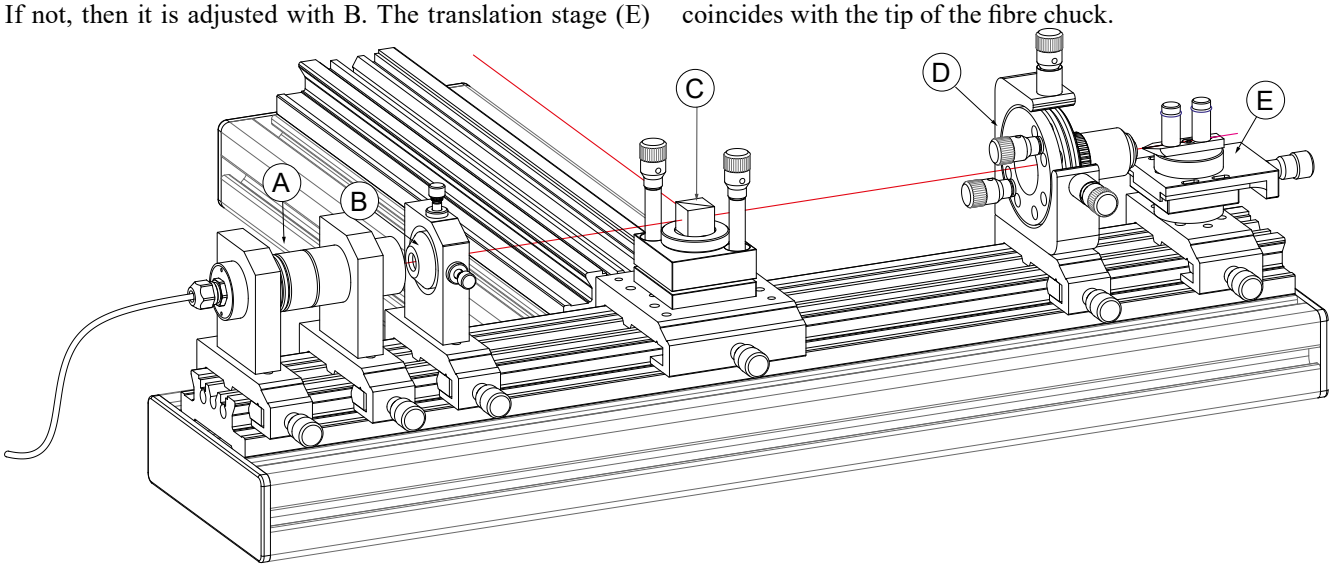

Fig. 60: Installation of the fibre holder

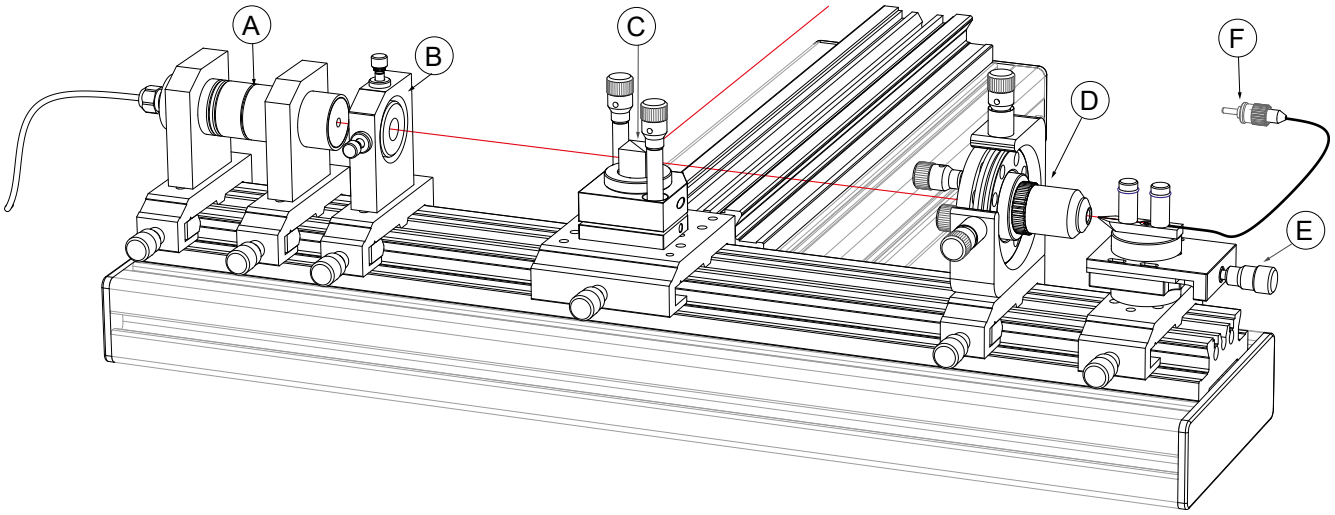

Fig. 61: Insertion of the pig tailed fibre patch cable (F)

4.3 Launching of the light into the fibre

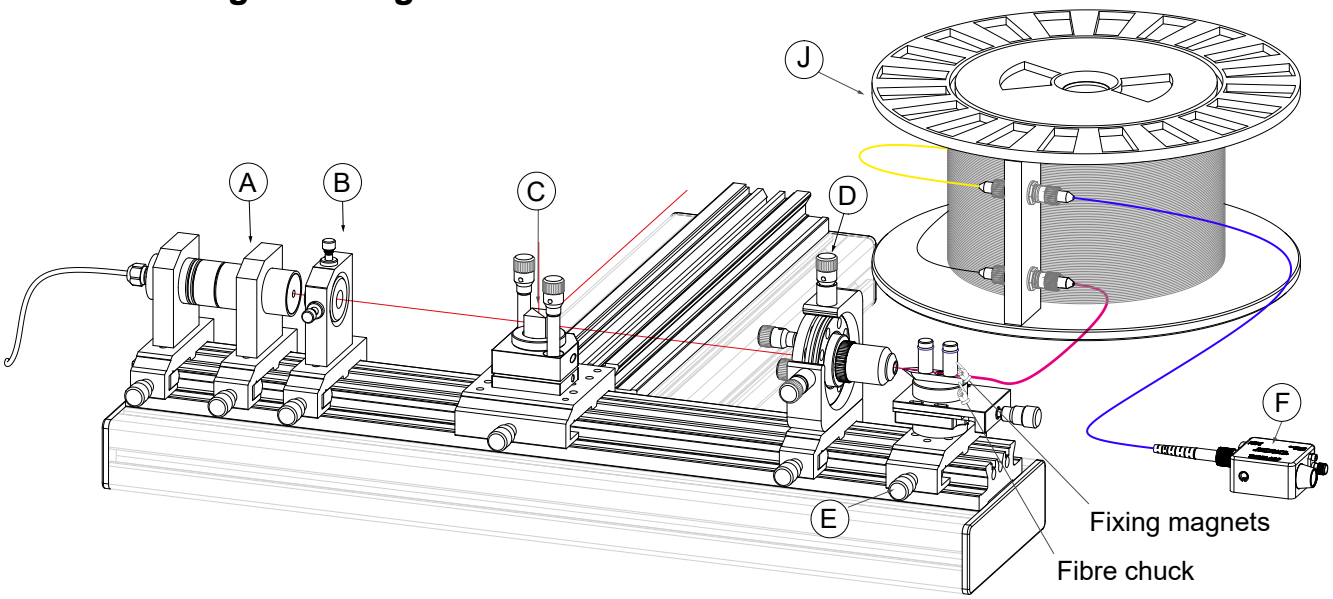

Fig. 62: Launching of the light into the fibre

After careful preparation of the pig tailed fibre end the bare part is inserted into the fibre chuck and fixed by means of the fixing magnets. The photodetector module (F) is connected with the ST/FC fiber patch cable and the output is connected to the oscilloscope with the provided SMA-BNC cable. One channel of the Oscilloscope is connected to the reference synchronisation signal of the control unit. This channel serves as a trigger for the expected signal from the fibre.
Now one switches the diode laser on and selects the repetition rate such that a flicker-free picture of the reference signal is displayed on the oscilloscope. A signal of the exiting light from the fibre spool (J) should be observed. If not, one adjusts the entry side of the fibre with the help of the translation stage towards or apart from the microscope objective. After a signal is observed, the adjustment of the coupling optics is further optimized. The position of the fibre entrance must be also be optimized with respect to the focus. After this adjustment has been made, the detector (G) is placed to its position (Fig. 63) and optimized. Observe the effects through the moving of the imaging optics (H) and also by the adjustment of the beam splitter cube (E). Optimise for highest signal intensity.

4.4 Detection and recording the back scattered light

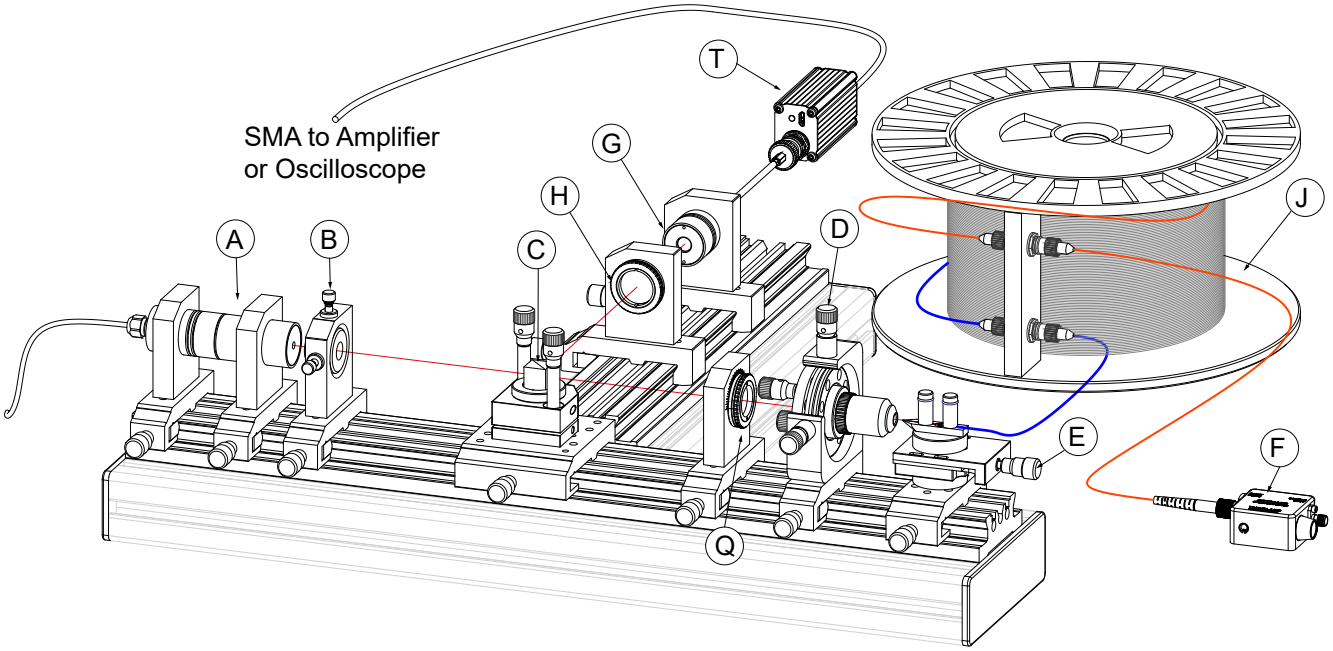

Fig. 63: Final setup to measuring the losses

As soon as the photodetector (G) is connected, a signal will be present. Because the polarisation of the diode laser and the polarising beam splitter (C) is not perfect, a small amount of the emitted intensity is reflected to the photodetector (G) via the focusing lens (C). It is used to align the beam splitter and the distance of the focusing lens (H) to the detector (G). In addition back reflected light from the surfaces of the quarter wave plate (Q), the coupling optics and the face surface of the fibre. Blocking the path between (C) and (Q) this effect can be determined.
The first measurement is taken on the digital storage oscilloscope according to Fig. 64, and if possible the data is finally taken onto a computer.

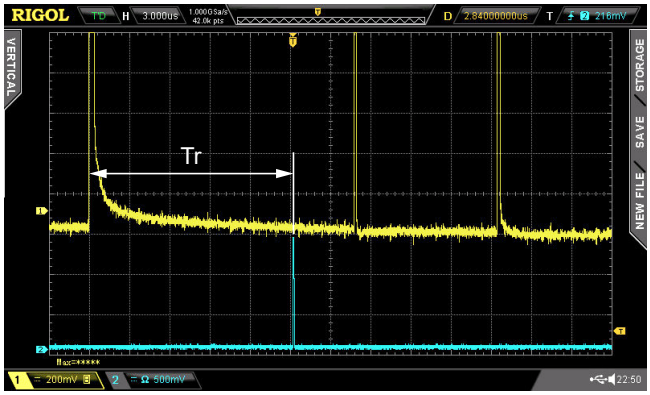

Fig. 64: Example of measurement

In this example we use a 2000 m and a 1000 m optical fibre in sequence. The blue track shows the signal at the ned of the fibres taken with the detector F, a transit time of 5.04 cm or 15.12 µsec is determined. With this the entire length L of the fibres is:

$$L = \frac{c}{n} \cdot Tr = \frac{3 \cdot 10^8}{1.46} \cdot 15.12 \cdot 10^{-6} = 3.107\ m$$

The actual length of each fibre is mentioned by the manufacturer statement on each drum. The value for the refractive index n=1.46 originates from the manufacturer.
The yellow curve shows the back scattered light which has been recorded with the second photodetector (G). The first peak is the start, the second the reflection of the end face of the 2000 m and the third peak the reflection of the 1000 m fiber.

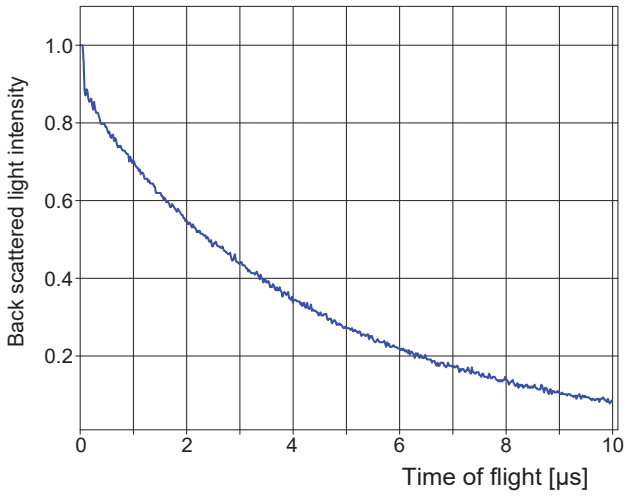

Fig. 65: Transitory course of the scattering light after switching off of the light impulse.

It is recommended to create from the oscilloscope tracks a data file. This allows to cut out the interesting part and apply a smoothing as shown in Fig. 65. Back scattered light, which is produced at points distanced from the entrance surface experience a higher attenuation mainly through losses. Therefore, the exponential part of the curve contains the information about the fibre loss. For the evaluation now, we put the returning intensity logarithmically in a new diagram.

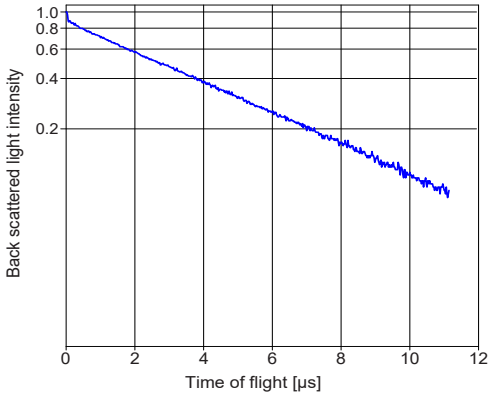

Fig. 66: The same measured values like in Fig. 65, however with logarithmically division of the ordinate

In the next step of evaluation, we concentrate on the linear part whose slope contains the loss or attenuation coefficient. This is represented in the following figure.

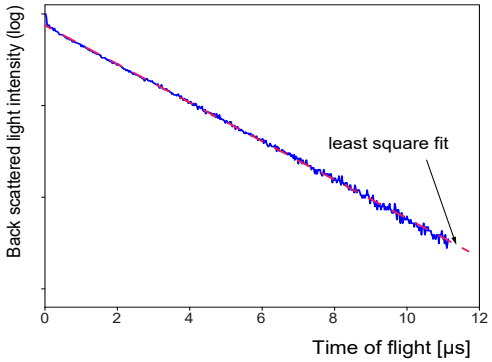

Fig. 67: Determination of the loss coefficient

Starting from the relationship:

$$I = I_0 \cdot e^{-\alpha \cdot t} \text{ or } \ln I = \ln I_0 - \alpha \cdot t\,,$$

in this example, through linear regression of the slope we get the value of α=4.45 dB/km. Normally the value of attenuation is given in dB/km which one gets through the following equation

$$\alpha_{dB} = 10 \cdot \log\left(\frac{I}{I_0}\right) = 10 \cdot \log\left(e^{-\alpha_L}\right)$$

With the assessment for the attenuation, it can be further noticed that the scattering light is produced at a location z in the fibre from a primary light intensity which has already become weak through previous attenuation. Fig. 67 includes both the parts. The correction results from the following consideration: The primary light is already attenuated at a location z according to:

$$I(z) = I_0 \cdot e^{-\alpha \cdot z}$$

I(z) is the primary light intensity for the scattering process at the location z and leads to scattering light which covers the way z to the fibre entrance. On the way it however, experiences an attenuation according to:

$$I(z=0) = I(z) \cdot \sigma_R \cdot e^{-\alpha \cdot z}$$

or

$$I(z=0) = I_0 \cdot \sigma_R \cdot e^{-2 \cdot \alpha \cdot z}$$

σ_R is a coefficient which denotes the efficiency of the scattering process whose value is not needed to be known for the determination of the attenuation.

5.0 Laser safety

The experimental system contains a pulse diode laser which is only suitable for laboratory applications.

With the individual modules in the assembled state, laser radiation (semiconductor laser) can be produced at 905 ± 10 nm with a maximum peak power of 70 W. The pulse width is 100 ns resulting in a pulse energy of 7 µJ. The maximum repetition rate is 2.5 kHz with a duty cycle of 1% resulting in an average power of 0.2 mW

The complete assembled laser is therefore a product which exhibits the power characteristics of a Class 3B laser. Since the OTDR is a laser system formed from combined modular elements and can therefore be modified in a number of different ways, the operator of this system must ensure that the safety requirements are maintained.
The manufacturer only provides a guarantee for the individual modules, but does not accept any responsibility for cases of damage which arise due to the combination of the modules. The user must observe the laser safety regulations, e.g. **DIN VDE0837 or IEC 0837**.

In these guidelines of February 1986 the following points are listed for the operation of laser equipment in laboratories and places of work.

Laser equipment in laboratories and places of work

Class 3B laser equipment

Class 3B lasers are potentially hazardous, because a direct beam or a beam reflected by a mirror can enter the unprotected eye (direct viewing into the beam). The following precautions should be made to prevent direct viewing into the beam and to avoid uncontrolled reflections from mirrors:

a.) The laser should only be operated in a supervised laser area

b.) Special care should be taken to avoid unintentional reflections from mirrors

c.) Where possible the laser beam should terminate on a material which scatters the light diffusely after the beam has passed along its intended path. The colour and reflection properties of the material should enable the beam to be diffused, so keeping the hazards due to reflection as low as possible.

Note: Conditions for safely observing a diffuse reflection of a Class 3B laser which emits in the visible range are :
Minimum distance of 13 cm between screen and cornea of the eye and a maximum observation time of 10 s. Other observation conditions require comparison of the radiation density of the diffused reflection with the MZB value.

d.) Eye protection is necessary if there is a possibility of either direct or reflected radiation entering the eye or diffuse reflections can be seen which do not fulfil the conditions in c.).

e.) The entrances to supervised laser areas should be identified with the laser warning symbol

MZB means Maximum Permissible Radiation (Maximal zulässige Bestrahlung) and it is defined in section 13 of DIN/VDE 0837.
Special attention is drawn to point 12.4 of DIN VDE0837:

Laser equipment for demonstration, display and exhibition purposes

Only Class 1 and Class 2 lasers should be used for demonstrations, displays and exhibitions in unsupervised areas. Lasers of a higher class should then only be permitted if the operation of the laser is controlled by an experienced and well trained operator and/or the spectators are protected from radiation exposure values which does not exceed the applicable MZB values.

Each laser system, which is used in schools for training etc. should fulfil all the applicable requirements placed on class 1 and class 2 laser equipment; also, it should not grant persons access to radiation which exceeds the applicable limits in Class 1 or Class 2.